(3) WL-TR-89-37

AD-A213 938

NONLINEAR OPTICAL MATERIAL STUDIES

M. O. Scully, et al

University of New Mexico
Center for Advanced Studies
800 Yale Blvd NE
Albuquerque, NM 87131

September 1989

Final Report

DTIC
ELECTE
OCT 2 4 1989
S D
D

Approved for public release; distribution unlimited.

Weapons Laboratory
Air Force Systems Command
Kirtland Air Force Base, NM 87117-6008

89 10 23 085

This final report was prepared by the Center for Advanced Studies at the University of New Mexico, Albuquerque, New Mexico, under contract F29601-87-C-0059 Job Order 33261B16 with the Weapons Laboratory, Kirtland Air Force Base, New Mexico. First Lieutenant Paul A. Laferriere (AROM) was the Laboratory Project Officer-in-Charge.

When Government drawings, specifications, or other data are used for any purpose other than in connection with a definitely Government-related procurement, the United States Government incurs no responsibility or any obligation whatsoever. The fact that the Government may have formulated or in any way supplied the said drawings, specifications, or other data, is not to be regarded by implication, or otherwise in any manner construed, as licensing the holder, or any other person or corporation; or as conveying any rights or permission to manufacture, use, or sell any patented invention that may in any way be related thereto.

This report has been authored by a contractor of the United States Government. Accordingly, the United States Government retains a nonexclusive, royalty-free license to publish or reproduce the material contained herein, or allow others to do so, for the United States Government purposes.

This report has been reviewed by the Public Affairs Office and is releasable to the National Technical Information Service (NTIS). At NTIS it will be available to the general public, including foreign nationals.

If your address has changed, if you wish to be removed from our mailing list, or if your organization no longer employs the addressee, please notify WL/AROM, Kirtland AFB, NM 87117-6008 to help us maintain a current mailing list.

This report has been reviewed and is approved for publication.

Paul A. Laferriere

PAUL A. LAFERRIERE
First Lieutenant, USAF
Project Officer

FOR THE COMMANDER

ANTONIO CORVO
Major, USAF
Chief, Quantum Optics Branch

HARRO ACKERMANN
Lieutenant Colonel, USAF
Chief, Optics Division

DO NOT RETURN COPIES OF THIS REPORT UNLESS CONTRACTUAL OBLIGATIONS OR NOTICE ON A SPECIFIC DOCUMENT REQUIRES THAT IT BE RETURNED.

UNCLASSIFIED
SECURITY CLASSIFICATION OF THIS PAGE

REPORT DOCUMENTATION PAGE

Form Approved OMB No. 0704-0188

1a. REPORT SECURITY CLASSIFICATION: Unclassified	1b RESTRICTIVE MARKINGS
2a. SECURITY CLASSIFICATION AUTHORITY	3. DISTRIBUTION/AVAILABILITY OF REPORT: Approved for public release; distribution unlimited.
2b. DECLASSIFICATION/DOWNGRADING SCHEDULE	
4 PERFORMING ORGANIZATION REPORT NUMBER(S)	5. MONITORING ORGANIZATION REPORT NUMBER(S): WL-TR-89-37
6a. NAME OF PERFORMING ORGANIZATION: Center for Advanced Studies, University of New Mexico / 6b. OFFICE SYMBOL (If applicable)	7a. NAME OF MONITORING ORGANIZATION: Weapons Laboratory
6c. ADDRESS (City, State, and ZIP Code): 800 Yale Blvd NE, Albuquerque, New Mexico 87131	7b. ADDRESS (City, State, and ZIP Code): Kirtland Air Force Base, New Mexico 87117-6008
8a. NAME OF FUNDING/SPONSORING ORGANIZATION / 8b. OFFICE SYMBOL (If applicable)	9 PROCUREMENT INSTRUMENT IDENTIFICATION NUMBER: F29601-87-C-0059
8c. ADDRESS (City, State, and ZIP Code)	10 SOURCE OF FUNDING NUMBERS

PROGRAM ELEMENT NO.	PROJECT NO.	TASK NO	WORK UNIT ACCESSION NO
62601F	3326	1B	16

11. TITLE (Include Security Classification): NONLINEAR OPTICAL MATERIAL STUDIES

12. PERSONAL AUTHOR(S): Scully, M. O.; Bergou, J.; Becker, W.; and McIver, J. K.

13a. TYPE OF REPORT	13b. TIME COVERED	14. DATE OF REPORT (Year, Month, Day)	15. PAGE COUNT
Final	FROM Sep 87 TO Sep 88	1989, September	52

16. SUPPLEMENTARY NOTATION

17. COSATI CODES			18. SUBJECT TERMS (Continue on reverse if necessary and identify by block number)
FIELD	GROUP	SUB-GROUP	Nonlinear Optical Materials, Nonlinear Waveguides, (162)
12	01		

19. ABSTRACT (Continue on reverse if necessary and identify by block number)

This report covers research on nonlinear optics theory. An analytical theory of the reflection and transmission of light from nonlinear optical interfaces is described. The general theory is applied to some simple two-dimensional nonlinear waveguide configurations. The intensity dependence of total versus differential ionization rates in laser-induced above-threshold ionization is also discussed.

20. DISTRIBUTION/AVAILABILITY OF ABSTRACT	21. ABSTRACT SECURITY CLASSIFICATION
☒ UNCLASSIFIED/UNLIMITED ☐ SAME AS RPT. ☐ DTIC USERS	Unclassified

22a. NAME OF RESPONSIBLE INDIVIDUAL	22b TELEPHONE (Include Area Code)	22c. OFFICE SYMBOL
Lieutenant Paul Laferriere	(505) 844-0475	WL/AROM

DD Form 1473, JUN 86 — Previous editions are obsolete.

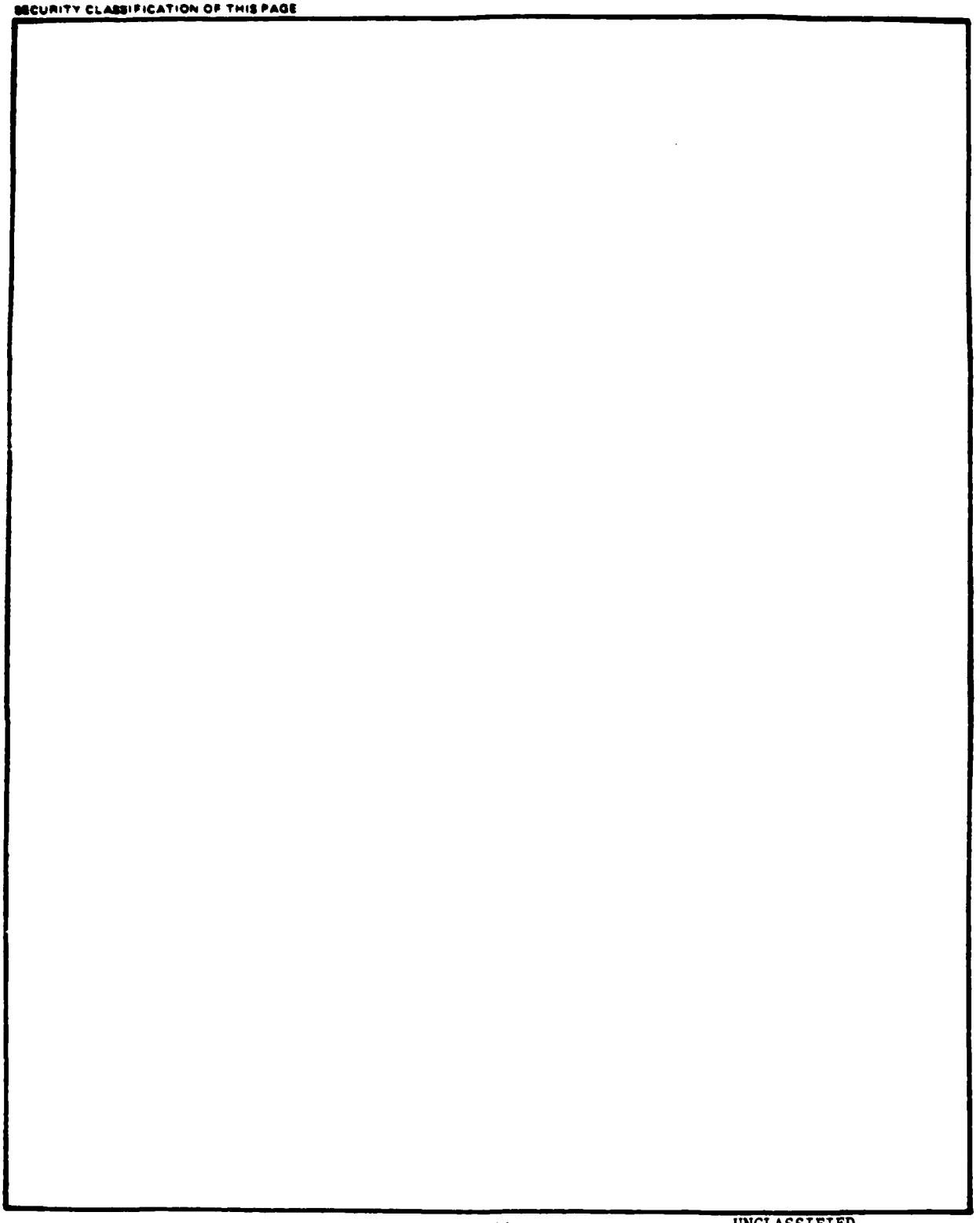

ACKNOWLEDGMENTS

The authors enjoyed useful discussions with R. R. Schlicher. J. Bergou is grateful to the Alexander von Humboldt-Foundation for providing a research fellowship at the Max-Planck-Institut fur Quantenoptik (Garching, FRG), where this work in Section 3 was initiated.

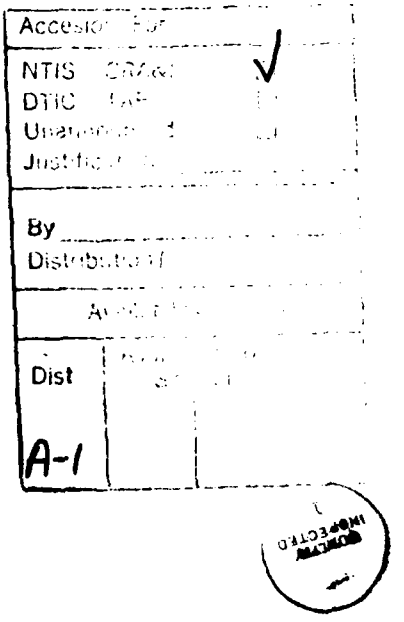

CONTENTS

1. WORK OVERVIEW

The first section in this report serves as a brief overview of the work. The second section describes an analytical theory of the reflection and transmission of light from nonlinear optical interfaces. The third section presents an application of the general theory to some simple nonlinear waveguide configurations. The last section deals with a very important aspect of above-threshold ionization, namely, the intensity dependence of total versus differential ionization rates.

1.1 GENERALIZATION OF THE LAWS OF REFRACTION AND REFLECTION FOR A NONLINEAR INTERFACE

We have generalized Snell's and Fresnel's formulas of reflection and refraction for the case of a nonlinear interface. We have explicitly dealt with the case when a plane wave is incident from a linear medium onto an interface with a medium of Kerr-type nonlinearity. We have investigated an incident transverse electric (TE) polarized wave, positive nonlinearity constant in the nonlinear medium, and totally reflecting interface at low incident intensity.

Our results can be summarized as follows. We could show that the solutions of the nonlinear wave equation, describing stationary behavior, fall into three categories:

1.1.1 Uniform phase wave. The amplitude is inhomogeneous, depending explicitly on the position in the nonlinear medium. This wave plays a crucial role in the regime of total internal reflection (TIR).

1.1.2 Uniform amplitude wave. The phase is that of a plane wave, but with wave vector depending on the intensity. This wave is excited in the nonlinear (NL) medium in the entire regime outside that of TIR, and also above a certain intensity threshold in the regime of TIR.

1.1.3 Inhomogeneous phase and amplitude waves. These waves play some role in a small part of the TIR regime and at extremely high incident intensities. Therefore, they are hard to observe, and nonstationary phenomena will probably be highly competing. By matching the above nonlinear waves with the linear incident and reflected waves at the boundary, we managed to generalize Fresnel's and Snell's formulas for the case under consideration. Outside the regime of TIR (incident angle $\theta_i < \theta_c$, where θ_c is the critical angle for TIR) the usual Fresnel's and Snell's formulas hold with the index of refraction in the NL medium being the actual intensity-dependent expression. In the regime of TIR, $\theta_c < \theta_i < \pi/2$, we defined a second critical angle θ_0. In the interval $\theta_c < \theta_i < \theta_0$ TIR is maintained up to a certain, relatively low, incident intensity I_0. Above this

threshold TIR is lost and normal reflection and refraction takes place. The nonlinear evanescent waves of 1.1.1 go continuously over into the NL radiation wave of 1.1.2. We derived explicit expressions for the phase shift and reflectivity associated with phenomena in this $\theta_c < \theta_i < \theta_0$ interval, both for $I < I_0$ and $I > I_0$.

In the interval $\theta_0 < \theta_i < \pi/2$, TIR is maintained up to a relatively high incident intensity I_0. Above this threshold TIR is lost and, since the inhomogeneous waves of 1.1.3 are extremely sensitive to small perturbations, nonstationary phenomena (i.e., generation of pulses) take place.

1.2 INTRINSIC PROPERTIES OF NONLINEAR TE WAVES GUIDED BY A SYMMETRIC SLAB

We have shown, by an appropriate scaling of parameters characterizing the nonlinear TE guided modes of a symmetric slab (linear core embedded between two identical media with Kerr nonlinearity), that their mutual dependence (dispersion relations) can be given by particularly simple expressions. This permits us to determine the range of variation of these parameters and the conditions for the appearance of asymmetric waves and surface modes. It also hints at the possibility of bistable switching with hysteresis between different branches of the dispersion curves.

1.3 INTENSITY DEPENDENCE OF TOTAL VERSUS DIFFERENTIAL IONIZATION RATES IN ABOVE-THRESHOLD IONIZATION

Above-threshold ionization (ATI) refers to the ionization of an atom by an intense laser field, such that the ejected electron absorbs more laser photons than is necessary for ionization. The energy spectrum of the ejected electrons thus consists of separate peaks corresponding to the absorption of 0, 1, 2, ... photons beyond the minimum number. The heights of the peaks, i.e., the partial ionization rates, are strongly dependent on the intensity of the laser field. For fields with an intensity $> 10^{13}$ W/cm^2 their intensity dependence can no longer be explained in terms of perturbation theory with respect to the laser field. In contrast, the total ionization rate, i.e., the sum of all the partial rates, is strictly proportional to I^N with N the minimum number of photons which have to be absorbed for ionization. This striking behavior has been observed in all pertinent experiments up to $I > 10^{14}$ W/cm^2. It is also exhibited in computer simulations for the hydrogen atom. The same phenomenon has also been observed (theoretically) in nuclear beta decay in an intense laser field, where the total decay rate is unaffected by the field

up to the critical field strength, while the differential rates are already dramatically distorted by fields which are less intense by ten orders of magnitude. In both cases, this phenomenon is due to the fact that the ionization or decay takes place much like a two-step process. The first step is the actual ionization or decay, while the second step is a final-state interaction between the laser field and the ejected electron, in the process of which the electron energy is redistributed. We have started, based on previous experience with nuclear beta decay, to attempt to justify this two-step assumption from first principles. In particular, we want to find out up to what intensity the I^N dependence will persist.

These specific areas of investigation are described in detail in the following sections.

2. GENERALIZATION OF THE LAWS OF REFRACTION AND REFLECTION FOR A NONLINEAR INTERFACE

2.1 INTRODUCTION

We derive a wave equation describing stationary phenomena along the interface. The solution in the linear medium is the usual plane-wave one. We show that in the NL medium the solutions fall into three categories: (a) waves with a constant phase (nonlinear evanescent waves), (b) waves with constant amplitude (nonlinear plane waves), and (c) waves with nonuniform amplitude and phase. From the boundary conditions (matching the tangential components of the electric and magnetic fields at the interface), we obtain the NL generalization of the Fresnel formulas. The implication is the following.

Let n_1 stand for the index of refraction in the linear medium ($\epsilon_1 = n_1^2$ is the dielectric constant) and n_2 the linear part of the index of refraction in the nonlinear medium ($\epsilon_2 = n_2^2$ is the linear dielectric constant in the NL medium). If $n_2 > n_1$, then in the entire interval $0 < \theta < \pi/2$ of angles of incidence θ (θ is measured from the interface and not from the normal to it), the waves in the NL medium are the nonlinear plane waves and the phenomenon is very similar to the phenomenon at a linear interface. In particular, everywhere in Fresnel's and Snell's formulas ϵ_2 should be replaced by the intensity-dependent expression $\epsilon_2 + \alpha|E_2|^2$ (α nonlinearity constant, E_2 amplitude in the NL medium). If $n_2 < n_1$ then in the $\theta_c < \theta < \pi/2$ interval ($\cos^2\theta_c = \epsilon_2/\epsilon_1$), the situation is similar to the $n_2 > n_1$ case. In the interval $0 < \theta < \theta_c$, TIR is possible up to a certain critical intensity $I_{cr} = I_{cr}(\theta)$.

Our main conclusion is that in this interval there exists a second critical angle θ_0 ($\sin^2\theta_0 = \frac{1}{2}\sin^2\theta_c$ or approximately $\theta_0 \simeq \theta_c/\sqrt{2}$), such that in the interval $\theta_0 < \theta < \theta_c$ the nonlinear evanescent waves exist up to a certain critical intensity I_{cr}, and at this intensity they go continuously over into the nonlinear plane waves; i.e., in this interval the critical intensity (upper limit) of TIR coincides with the threshold intensity I_{th} (lower limit) of the nonlinear plane waves. In the $0 < \theta < \theta_0$ interval, however, $I_{cr} > I_{th}$, and in the intensity range $I_{th} < I < I_{cr}$ both waves are possible. Which one of them will exist at a given intensity depends on the past of the system (hysteresis in the reflection as a function of intensity being one possible consequence). A linear stability analysis confirms these findings and leaves no room for the nonuniform amplitude and phase waves. Thus, their existence requires further study.

2.2 GEOMETRY, WAVE EQUATION, BOUNDARY CONDITIONS

We deal with the geometry described in the following.

A plane wave with amplitude E_0 is incident on the interface between a linear medium (dielectric constant ϵ_1) and a nonlinear medium with Kerr-type nonlinearity (dielectric function $\epsilon_2 + \alpha|E_2|^2$). The wave is incident from the linear medium, its amplitude is E_0 and the angle of incidence is θ. The amplitude of the reflected wave is rE_0; r is the reflection coefficient. The incident, reflected and refracted waves are all polarized perpendicularly to the plane of incidence, along the y-axis (TE polarization). The amplitude of the transmitted wave is E_2.

According to the assumption about TE polarization, we look for the electric field $\vec{E}$ and magnetic field $\vec{H}$ in the form

$$\vec{E} = (0, E(x), 0)e^{i(\beta z - \omega t)}; \quad \vec{H} = (H_x(x), 0, H_z(x))e^{i(\beta z - \omega t)} \tag{1}$$

Here ω is the frequency and β is the propagation constant, related to the wave number in vacuum $k = \omega/c$, index of refraction $n_1 = \sqrt{\epsilon_1}$, and angle of incidence θ as $\beta^2 = k^2\epsilon_1 \cos^2\theta$.

Obviously div $\vec{E} = 0$. From curl $\vec{E} = -\frac{1}{c}\frac{\partial \vec{H}}{\partial t}$ we obtain

$$H_x = -(\beta/k)E; \quad H_z = -(i/k)\frac{dE}{dx} \tag{2}$$

Using these equations one can see that div $\vec{H} = 0$ is automatically satisfied. From curl $\vec{H} = \frac{\epsilon}{c}\frac{\partial \vec{E}}{\partial t}$ we obtain

$$i\frac{dH_x}{dx} + k\epsilon E + \beta H_z = 0 \tag{3}$$

with

$$\epsilon = \begin{cases} \epsilon_1, & \text{if } x < 0 \\ \epsilon_2 + \alpha|E_2|^2, & \text{if } x > 0 \end{cases} \tag{4}$$

Using Equation 2 in Equation 3, we can eliminate H_x and H_z and obtain

$$\frac{d^2E}{dx^2} + [k^2\epsilon - \beta^2]E = 0 \tag{5}$$

which is our starting equation.

Boundary conditions require continuity of the tangential components of the electric and magnetic fields at the interface, $x = 0$, i.e., continuity of E_y and H_z. In view of Equations 1 and 2, this means

$$E \text{ and } E' \text{ continuous at } x = 0 \tag{6}$$

Equations 5 and 6, together with the definition of k, ϵ, and β, form the basis of the theory.

2.3 SOLUTION OF THE WAVE EQUATION IN THE DIFFERENT REGIONS

2.3.1 *Solution in the Linear Medium*

From Equation 4 we find that in the linear medium $(x < 0)\epsilon = \epsilon_1$. Using this in Equation 5 yields

$$E'' + k_1^2 E = 0 \tag{7}$$

with

$$k_1^2 = k^2\epsilon_1 - \beta^2 = k^2\epsilon_1 \sin^2\theta \tag{8}$$

k_1 is just the x component of the full wave vector $k\sqrt{\epsilon_1}$. The solution can be written as the sum of an incident and a reflected plane wave:

$$E(x) = E_0 e^{ik_1 x} + rE_0 e^{-ik_1 x}, \quad x < 0 \tag{9}$$

where E_0 is the amplitude of the incident plane wave and r is the reflection coefficient.

2.3.2 *Solution in the Nonlinear Medium*

From Equation 4 we find that in the nonlinear medium $(x > 0)\epsilon = \epsilon_2 + \alpha|E|^2$. Using this in Equation 5, we find

$$E'' + [k^2\epsilon_2 - \beta^2]E + k^2\alpha|E|^2E = 0 \tag{10}$$

In the rest of this section we categorize the possible solutions of this equation.

2.3.2.1 *Uniform Phase Wave (Nonlinear Evanescent Wave)*

Assume that $E = E_2(x)e^{i\varphi}$ where E_2 is real. For this case

$$E_2'' - \gamma^2 E_2 + \alpha k^2 E_2^3 = 0 \tag{11}$$

where $\gamma^2 = \beta^2 - k^2\epsilon_2$. A first integral can be found by multiplying this equation with $E_2'(= \frac{dE_2}{dx})$. It is given by

$$(E_2')^2 - \gamma^2 E_2^2 + \frac{1}{2}\alpha k^2 E_2^4 = \text{const.} \tag{12}$$

For evanescent waves $\gamma^2 > 0$ (i.e., $\cos\theta > \cos\theta_c \equiv \sqrt{\frac{\epsilon_2}{\epsilon_1}}; 0 < \theta < \theta_c$) and both E_2 and $E_2' \to 0$ if $x \to \infty$, hence const = 0. It is then straightforward to integrate Equation 12 once again, yielding

$$E_2 = \pm\sqrt{\frac{2}{\alpha}}\frac{\gamma}{k}\frac{1}{\cosh[\gamma(x - x_0)]} \text{ or } E = E_2 e^{i\varphi} \tag{13}$$

Here x_0 is a constant of integration to be determined from the conditions of continuity. A constant phase and amplitude wave ($E_2' = E_2'' = 0$) can also be found from Equation 11 or Equation 12:

$$\alpha E_2^2 = \epsilon_1\cos^2\theta - \epsilon_2 \tag{14a}$$

or

$$\epsilon_1 \cos^2\theta = \alpha E_2^2 + \epsilon_2 \tag{14b}$$

This corresponds to an intensity which makes a given incident angle critical, the right-hand side of Equation 14b being the square of the effective index of refraction in the nonlinear medium.

Solutions of Equation 12 for an arbitrary constant can be expressed in the form of elliptic integrals. We come back to this in 2.3.2.3.

2.3.2.2. *Uniform Plane and Amplitude Wave*

Assume now that $E = E_2 e^{i(k_2 x + \varphi)}$ where $E_2 = \text{const}$. From Equation 10 we find that this is possible if

$$k_2^2 = k^2(\epsilon_2 + \alpha|E_2|^2) - \beta^2 \geq 0 \tag{15}$$

If $\epsilon_2 > \epsilon_1$, such a wave always exists. If $\epsilon_2 < \epsilon_1$, then for $\epsilon_1 \cos^2\theta < \epsilon_2 (\theta > \theta_c)$ such a wave exists always. If $\epsilon_1 \cos^2\theta > \epsilon_2 (\theta < \theta_c)$, then such a wave exists if $\alpha|E_2|^2 \geq \epsilon_1 \cos^2\theta - \epsilon_2 = I_{th}(\theta)$, i.e., if the intensity exceeds a certain threshold intensity. For $I = I_{th}$ we just reobtain the constant phase and amplitude wave of Equation 14a. The nonlinear plane wave can thus be written as

$$E = E_2 e^{i(k_2 x + \varphi)}, \quad x > 0 \tag{16}$$

where k_2 is the intensity-dependent wave vector as given by Equation 15, and E_2 is to be determined form the conditions of continuity.

2.3.2.3. *Nonuniform Plane and Amplitude Wave*

Assume that both the amplitude and phase are now functions of x, i.e.,

$$E(x) = E_2(x) e^{i\left|\int k_2(x)dx + \varphi\right|} \tag{17}$$

Substituting this into Equation 10 we can separate the real and imaginary parts of the wave equation, yielding

$$E_2'' - k_2^2 E_2 + (k^2\epsilon_2 - \beta^2 + k^2\alpha|E_2|^2)E_2 = 0 \tag{18}$$

from the real part, and

$$2k_2 E_2' + k_2' E_2 = 0 \tag{19}$$

from the imaginary part. Equation 19 can be integrated right away, giving

$$E_2^2 \cdot k_2 = \text{const} = c_1 \tag{20}$$

i.e., the expression on the left-hand side is an integral of motion. The solution in section 2.3.2.1 corresponds to $k_2 = \text{const} = 0$, and the solution in section 2.3.2.2. corresponds to both E_2 and $k_2 = \text{const}$. Using Equations 20 and 18 we can eliminate k_2 and obtain

$$E_2'' - \frac{c_1^2}{E_2^3} + [k^2\epsilon_2 - \beta^2 + k^2\alpha E_2^2]E_2 = 0 \tag{21}$$

Again, by multiplying Equation 21 with E_2' we can find a first integral in the form

$$(E_2')^2 + \frac{c_1^2}{E_2^2} + [k^2\epsilon_2 - \beta^2]E_2^2 + \frac{1}{2}k^2\alpha E_2^4 = c_2 \tag{22}$$

Equation 12 is a particular case when $c_1 = 0$. The solution of Equation 22 can again be reduced to elliptic integrals.

2.4 BOUNDARY CONDITIONS, FRESNEL'S AND SNELL'S FORMULAS

2.4.1 *The Case* $\epsilon_2 > \epsilon_1$

We can match an incident and reflected plane wave to a nonlinear plane wave in the entire $0 < \theta < \pi/2$ interval. Inserting Equations 9 and 16 into Equation 6, we obtain

$$E_0(1 + r) = E_2 e^{i\varphi} \tag{23}$$

from the continuity of E at $x = 0$ and

$$k_1 E_0 (1 - r) = k_2 E_2 e^{i\varphi} \tag{24}$$

from the continuity of E' at $x = 0$. By comparing the imaginary parts of Equations 23 and 24 we see that $\varphi = 0$, r = real. Using Equation 23 in Equation 24, we can eliminate E_2 from Equation 24 (note that k_2 also depends on E_2 in view of Equation 15), yielding

$$k_1 \frac{1 - r}{1 + r} = k_2 \tag{25}$$

If we take the square of this equation and use Equation 8 for k_1^2, and Equation 15 for k_2^2 (E_2 is substituted from Equation 23), then we obtain a fourth-order equation for r. It is, however, linear in the intensity parameter $I \equiv \alpha E_0^2/\epsilon_1$. We can therefore express I as a function of r, giving

$$I = -\frac{(r - r_0)(r - \frac{1}{r_0})}{(r + 1)^4} \left(\frac{\epsilon_2}{\epsilon_1} - 1 \right) \tag{26}$$

with

$$r_0 = \frac{\sin\theta - \sqrt{(\epsilon_2/\epsilon_1)^2 - \cos^2\theta}}{\sin\theta + \sqrt{(\epsilon_2/\epsilon_1)^2 - \cos^2\theta}} \tag{27}$$

We can now plot I as a function of r and invert this plot graphically to obtain $r = r(I, \theta, \epsilon_2, \epsilon_1)$. First we note that if $\alpha = 0$ (linear media on both sides of the interface) then $I = 0$, and from Equation 26 $r = r_0$ or $r = \frac{1}{r_0}$. Since $-1 < r_0 < 0$, the only physically meaningful solution is $r = r_0$. This is just Fresnel's formula for the reflection of a TE wave from a linear boundary. Furthermore, the r.h.s. of Equation 26 is positive if $-1 < r < r_0 < 0$, i.e., we have to plot Equation 26 only in this interval. The result is shown in Fig. 1. The reflection coefficient for low incident intensity coincides with that given by the (linear) Fresnel formula. With increasing intensity it decreases monotonically and approaches -1 as $I \to \infty$. The interface becomes less and less transparent as the intensity increases.

2.4.2 *The Case* $\epsilon_2 < \epsilon_1$

We can define a critical angle of incidence θ_c for which $\cos^2\theta_c = \frac{\epsilon_2}{\epsilon_1}$. In the linear case for $0 < \theta < \theta_c$ total internal reflection takes place and for $\frac{\pi}{2} > \theta > \theta_c$ ordinary reflection takes place. In the nonlinear case we see from Equation 15 that for $\theta > \theta_c$ the nonlinear plane waves exist for any I, whereas for $\theta < \theta_c$ they exist above a certain threshold intensity I_{th}. Also, from Section 2.3.2, the nonlinear evanescent waves exist in this interval, below a certain critical intensity I_c. Therefore we consider the $\theta > \theta_c$ and $\theta < \theta_c$ cases separately.

2.4.2.1 $\theta_c < \theta < \pi/2$

In this case much of the treatment of the previous subsection holds. In particular, Equation 26 can be rewritten for this case as

$$I = \frac{(r - r_0)(r - \frac{1}{r_0})}{(r+1)^4} \sin^2\theta_c \tag{28}$$

where r_0 is still given by Equation 27. Now $0 < \frac{1-\cos\theta_c}{1+\cos\theta_c} < r_0 < 1$ and the r.h.s. is positive if $r < r_0$. Again, for $I = 0$, the solution $r = r_0$ reproduces Fresnel's formula; otherwise we plot I in the interval $-1 < r < r_0$. The result is shown in Fig. 2. The reflection coefficient for low incident intensity coincides with that given by the (linear) Fresnel formula. With increasing intensity it decreases monotonically. The intensity $I = \sin^2\theta_c$ (i.e., $\epsilon_2 + \alpha E_0^2 = \epsilon_1$) makes the interface transparent, and the reflection is 0. If we increase the intensity further, the effective index of refraction becomes larger in the NL medium than in the linear one, and the behavior is similar to that found in Equation 23 for $\epsilon_2 > \epsilon_1$. Note that there is a phase change from 0 to π at this point.

2.4.2.2 $0 < \theta < \theta_c$

In this case the nonlinear evanescent waves and nonlinear plane waves may coexist. We treat them again separately.

2.4.2.2.1 *NL Plane Waves (NLPW)*

If $\epsilon_2 < \epsilon_1$ and $\theta < \theta_c$, then from Equation 15, we see that the NLPW exists above the threshold intensity I_{th} given by $k_2^2 = 0$. Using that $E_2 = (1 + r)E_0$ and at threshold $r = 1$, we obtain $(I_{th} = \alpha E_{0th}^2/\epsilon_1)$

$$I_{th} = \frac{\cos^2\theta - \cos^2\theta_c}{4}; \quad \left(0 < I_{th} < \frac{\sin^2\theta_c}{4}\right) \tag{29}$$

or

$$\epsilon_1 \cos^2 \theta = \epsilon_2 + \alpha(2E_0)^2_{th} \tag{30}$$

In other words, at the threshold intensity the given incident angle $\theta(0 < \theta < \theta_c)$ becomes critical in the sense that $\epsilon_1 \cos^2 \theta$ matches the intensity-dependent effective dielectric constant of the NL medium. If we increase the intensity further while keeping θ fixed, the condition of total internal reflection cannot be satisfied any more.

The continuity Equations 23 and 24 remain the same for this case and, consequently, Equation 28 also holds. The only difference is that r_0, as given by Equation 27, is just a phase factor, $r_0 = e^{-2i\varphi}$, where

$$\tan\varphi = \frac{\sqrt{\cos^2\theta - \cos^2\theta_c}}{\sin\theta} \tag{31}$$

Since these waves exist only above a threshold intensity, they do not have a linear limit. It is therefore more convenient to write Equation 28 for this case as

$$I = \frac{\cos^2\theta - \cos^2\theta_c}{(1+r)^2} + \frac{(1-r)^2}{(1+r)^4}\sin^2\theta \tag{32}$$

In Fig. 3 we plot this expression for a fixed $\theta(0 < \theta < \theta_c)$ as a function of r. The interpretation of $I = \sin^2\theta_c$ and the phase change going from $I < \sin^2\theta_c$ to $I > \sin^2\theta_c$ is the same as in 2.4.2.1.

2.4.2.2.2 *NL Evanescent Waves (NLEW)*

Using Equations 9 and 13 in the continuity Equation 6 we obtain

$$E_0(1+r) = \sqrt{\frac{2}{\alpha}}\frac{\gamma}{k}\frac{e^{i\varphi}}{\cosh(\gamma x_0)} \tag{33}$$

from the continuity of E, and

$$ik_1 E_0(1-r) = \sqrt{\frac{2}{\alpha}}\frac{\gamma^2}{k}\frac{e^{i\varphi}\tanh(\gamma x_0)}{\cosh(\gamma x_0)} \tag{34}$$

from the continuity of E' at $x = 0$. These are two complex equations to determine r (which is, in general, complex), φ and x_0 as a function of θ and E_0. Dividing Equation 34 by 33 we obtain

$$ik_1 \frac{1-r}{1+r} = \gamma \tanh(\gamma x_0) \tag{35}$$

or, expressing r from here, we get

$$r = \frac{k_1 + i\gamma \tanh(\gamma x_0)}{k_1 - i\gamma \tanh(\gamma x_0)} \tag{36}$$

Hence r is a phase factor with unit modulus. Comparing the phases of both sides of either Equation 33 or 34, we see that

$$r = e^{2i\varphi} \tag{37}$$

That is, the phase shift of the reflected wave is twice the phase shift of the transmitted wave, and $|r| = 1$, i.e., we have TIR where these waves exist.

If we use Equation 37 in Equations 33 and 35, and then eliminate x_0 from Equation 33 with the help of Equation 35, then we obtain a biquadratic equation for $\tan\varphi$. The solution yields

$$\tan^2\varphi = \frac{\sin^2\theta_c - 2\sin^2\theta \pm \sqrt{\sin^4\theta_c - 8I\sin^2\theta}}{2\sin^2\theta} \tag{38}$$

From this expression we infer the existence of a second critical angle θ_c defined as

$$\sin^2\theta_0 = \frac{1}{2}\sin^2\theta_c \tag{39a}$$

or, since usually θ_c is already a small angle, to a good approximation

$$\theta_0 \approx \theta_c/\sqrt{2} \tag{39b}$$

We deal with the intervals $\theta_0 < \theta < \theta_c$ and $0 < \theta < \theta_0$ separately.

- $\theta_0 < \theta < \theta_c$

In this case $\sin^2\theta_c - 2\sin^2\theta < 0$ and only the + sign in front of the square root in Equation 38 gives physical results. For $I = 0$, Equation 38 becomes identical with Equation 31 and reproduces the phase shift in total reflection for the linear case. We have two requirements: the expression under the square root in Equation 38 has to be nonnegative, which gives

$$I < \frac{\sin^4\theta_c}{8\sin^2\theta} \equiv I_1 \tag{40}$$

and the entire Equation 38 has to be nonnegative, which gives

$$I < \frac{\cos^2\theta - \cos^2\theta_c}{2} \equiv I_2 \tag{41}$$

Since $I_2 < I_1$, this means that the nonlinear evanescent waves in the $\theta_0 < \theta < \theta_c$ interval exist if

$$0 < I < I_2 \tag{42}$$

Furthermore, since $I_2 = 2I_{th}$, where I_{th} is given by Equation 29, in the interval $I_{th} < I < 2I_{th}$ the nonlinear evanescent waves and nonlinear plane waves coexist. In Fig. 4 we plot the phase of r for a fixed θ, as a function of I. The reflectivity $|r|$ is up to I_2. When this is viewed together with Fig. 4, it indicates the possibility of a hysteresis jump as shown in Fig. 7. One can increase the intensity to I_2 from 0 and have TIR. At this intensity TIR is lost and the reflectivity drops by a finite amount corresponding to this intensity in Fig. 3. If we now decrease the intensity along this line in Fig. 3, then at $I = I_{th}$ the reflectivity is 1 and we match the reflectivity $|r| = 1$. However, at this point (i.e., when TIR is restored), the phase jumps by a finite amount from 0 to a value given by Fig. 4 at $I = I_{th}$.

- $0 < \theta < \theta_0$

In this case $\sin^2\theta_c > 2\sin^2\theta$ and both signs in Equation 38 are possible. The solution with the + sign exists for $0 < I < I_1$, with I_1 given by Equation 41. The solution with

the - sign exists if Equation 38 and its discriminant are nonnegative, giving $I_2 < I < I_1$. Since $I_1 > I_{th}$, again the NLEW's and NLPW's coexist for $I_{th} < I < I_1$. In Fig. 5 we plot the phase of $r_\pm$ for a fixed θ as a function of I. The subscript $\pm$ corresponds to the choice of sign in Equation 38. Again, when this figure is viewed together with Fig. 3, it indicates the possibility of a hysteresis jump between the + branch and the NLPW when the intensity is increased. If it is decreased along the NLPW branch, it matches continuously to $|r_+|$, but now the phase jumps at both branching points. It does not seem to be easy to excite the − branch of Fig. 5.

Figure 6 summarizes the existence conditions on the $\theta - I$ plane. The different boundaries are given by $I_{th}(\theta), I_1(\theta)$, and $I_2(\theta)$. In region I the nonlinear evanescent wave (NLEW) of 2.4.2.2.2 exists. In region II the NLEW$_+$ (positive branch) of 2.4.2.2.2 exists. In region III the NLEW of 2.4.2.2.2 and the nonlinear plane wave (NLPW) of 2.4.2.2.1 coexist. In region IV the NLEW$_+$ of 2.4.2.2.2 and NLPW of 2.4.2.2.1 coexist. In region V the NLEW$_+$, NLEW$_-$ (negative branch) of 2.4.2.2.2 and the NLPW of 2.4.2.2.1 coexist. In region VI only the NLPW of 2.4.2.2.1 exists. Finally, in Fig. 8, we plot the critical angle as a function of the incident intensity as given by Equation 30. In the regions of coexistence (III, IV, V) one can expect bi- or multistability. Which of the above waves is actually stable requires further investigation.

A closing remark: If, instead of a coherent incident field, the interface is irradiated by an incoherent field, then the incident and reflected fields do not add in phase and the intensity at total reflection is not $4E_0^2$ at the interface, but only $2E_0^2$. This would increase the threshold intensity for the excitation of NLPW's from I_{th} to $2I_{th}$, which coincides with the cutoff intensity of NLEW's in the $\theta_0 < \theta < \theta_c$ region. Therefore, our expectation is that the observation of a hysteresis loop in the intensity-dependent reflectivity is almost impossible for $\theta_0 < \theta < \theta_c$. On the other hand, for $0 < \theta < \theta_0$ the observation is possible, since the cutoff intensity of the NLPW$_+$ branch $I_1 > 2I_{th}$.

2.5 REVIEW

We have defined a second critical angle θ_0 in the region of total internal reflection. If the angle of incidence θ is $\theta_0 < \theta < \theta_c$, then the evanescent waves become cut off at a certain intensity and go over into radiation waves in a continuous way. In the $0 < \theta < \theta_0$ region the reflectivity may exhibit hysteresis jumps as a function of intensity.

In the next section, as an application of this general theory, we investigate nonlinear guided waves in a symmetric slab configuration.

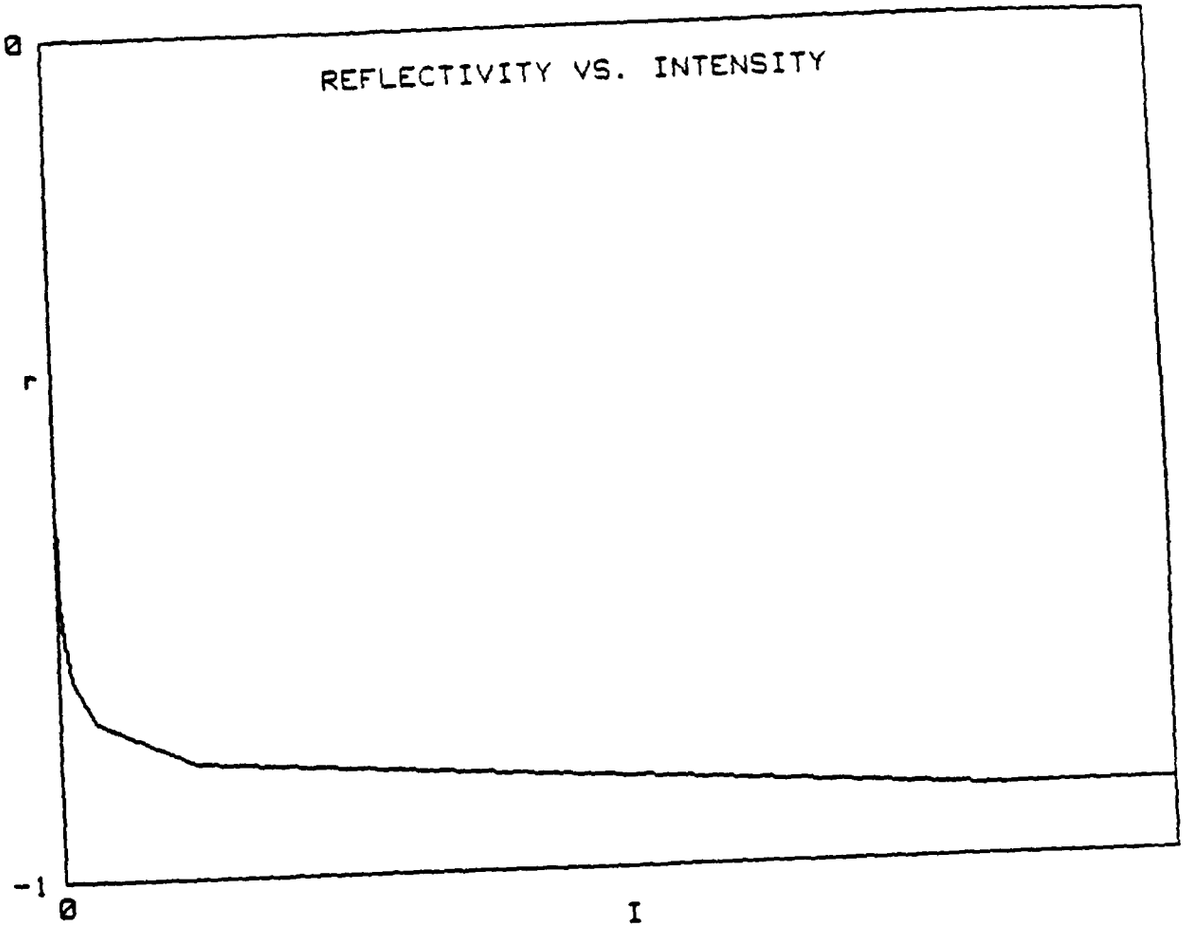

Fig. 1. Reflection coefficient r versus nonlinear intensity $I(\equiv \alpha E_0^2/\epsilon_1)$. (Here $\epsilon_1 = n_1^2 = (1.5)^2$ is the dielectric constant of the linear medium, $\epsilon = \epsilon_2 + \alpha|E|^2 = (1.6)^2 + \alpha|E|^2$ is the dielectric function of the nonlinear medium, α is the nonlinearity constant, E_0 is the amplitude of the incident field, E is the amplitude of the transmitted field. The plot corresponds to the analytical expression (26) for $\theta = 45°$. $I = \alpha E_0^2 \epsilon_1$ is in arbitrary units.)

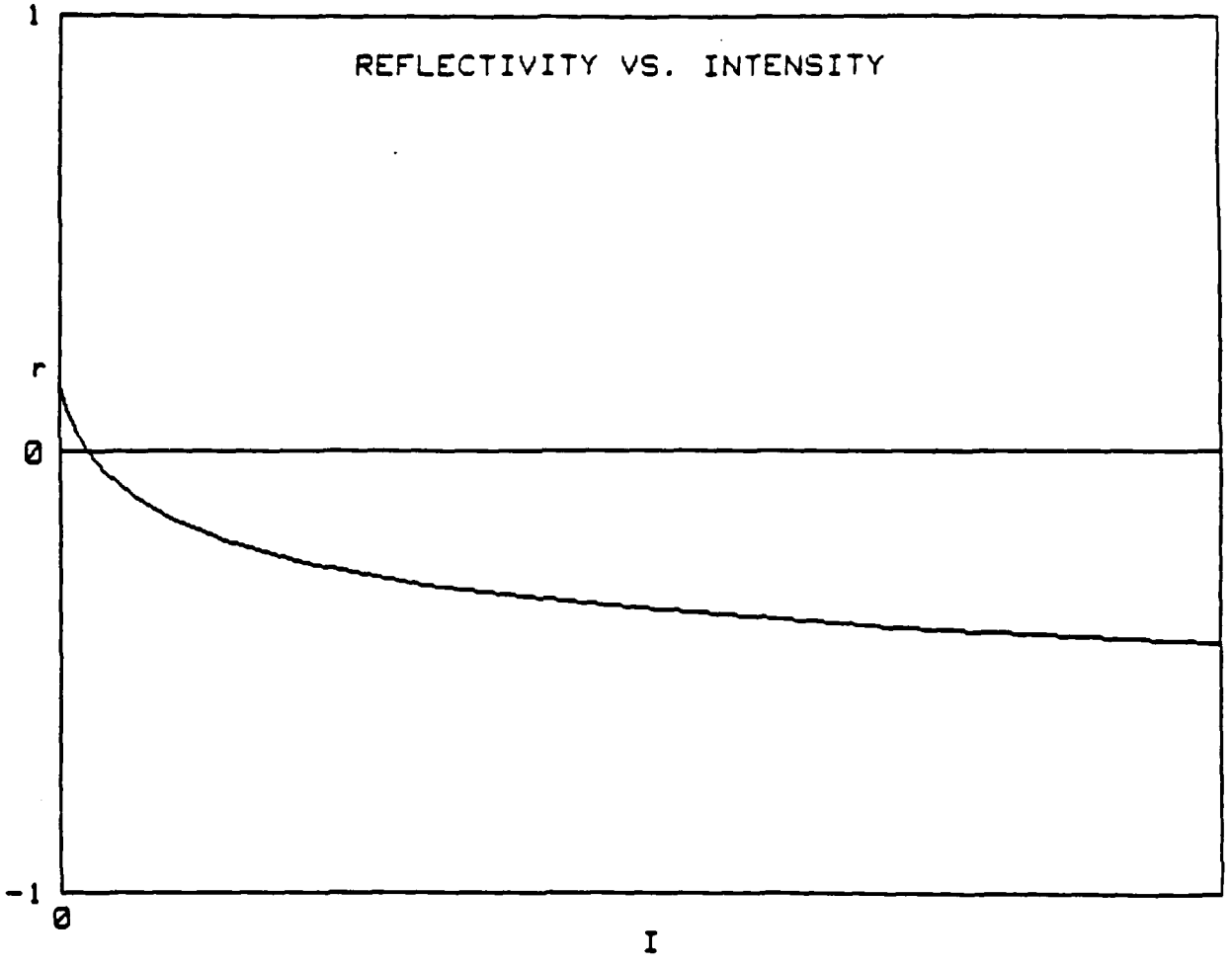

Fig. 2. Reflection coefficient r versus nonlinear intensity I. (The meaning of the parameters is the same as previously, but with $\epsilon_1 = (1.6)^2, \epsilon_2 = (1.5)^2$. There exists now a critical angle, $\cos^2 \theta_c = \epsilon_2/\epsilon_1$ or $\theta_c \approx 20°$, such that for $\theta > \theta_c$ normal reflection and for $\theta < \theta_c$ total reflection takes place. The plot corresponds to the analytical expression (28) for $\theta = 45°$.)

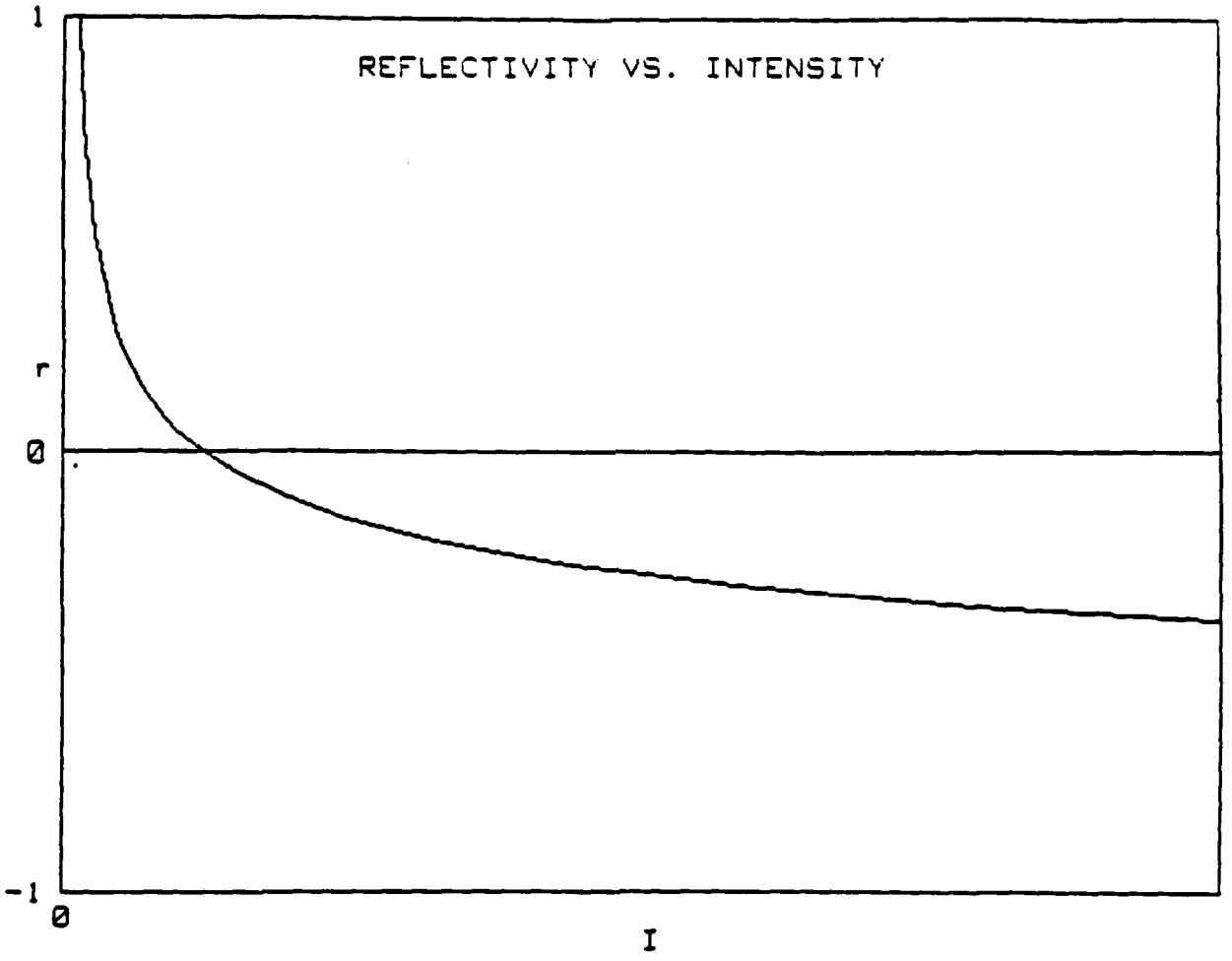

Fig. 3. Same as Fig. 2. but for $\theta = 15°$, i.e., in the total reflection interval. (The plot corresponds to the analytical expression (32) with $\theta = 15°$. Note that normal reflection occurs only above a threshold intensity I_{th} (given by (29)). This can be said differently: the critical angle, as given by (29) or (30), becomes intensity-dependent and total reflection, which takes place at low intensity, is replaced by ordinary reflection and refraction.)

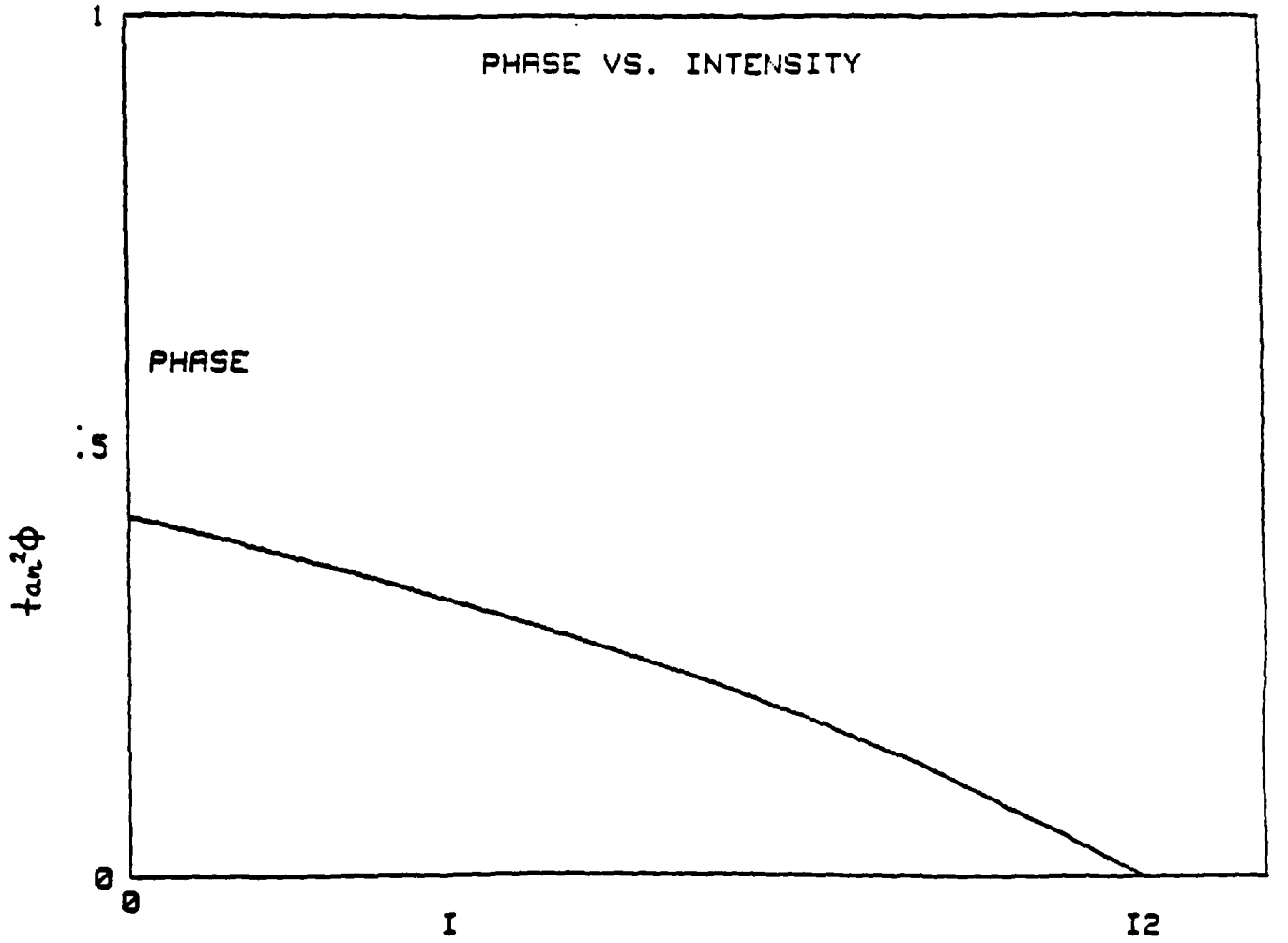

Fig. 4. $\mathrm{Tan}^2\phi$ versus the nonlinear intensity parameter I. (ϕ is the phase shift upon reflection. Parameter values are the same as in Fig. 3. The plot corresponds to Eq. (38) with the upper (+) sign in front of the square-root expression.)

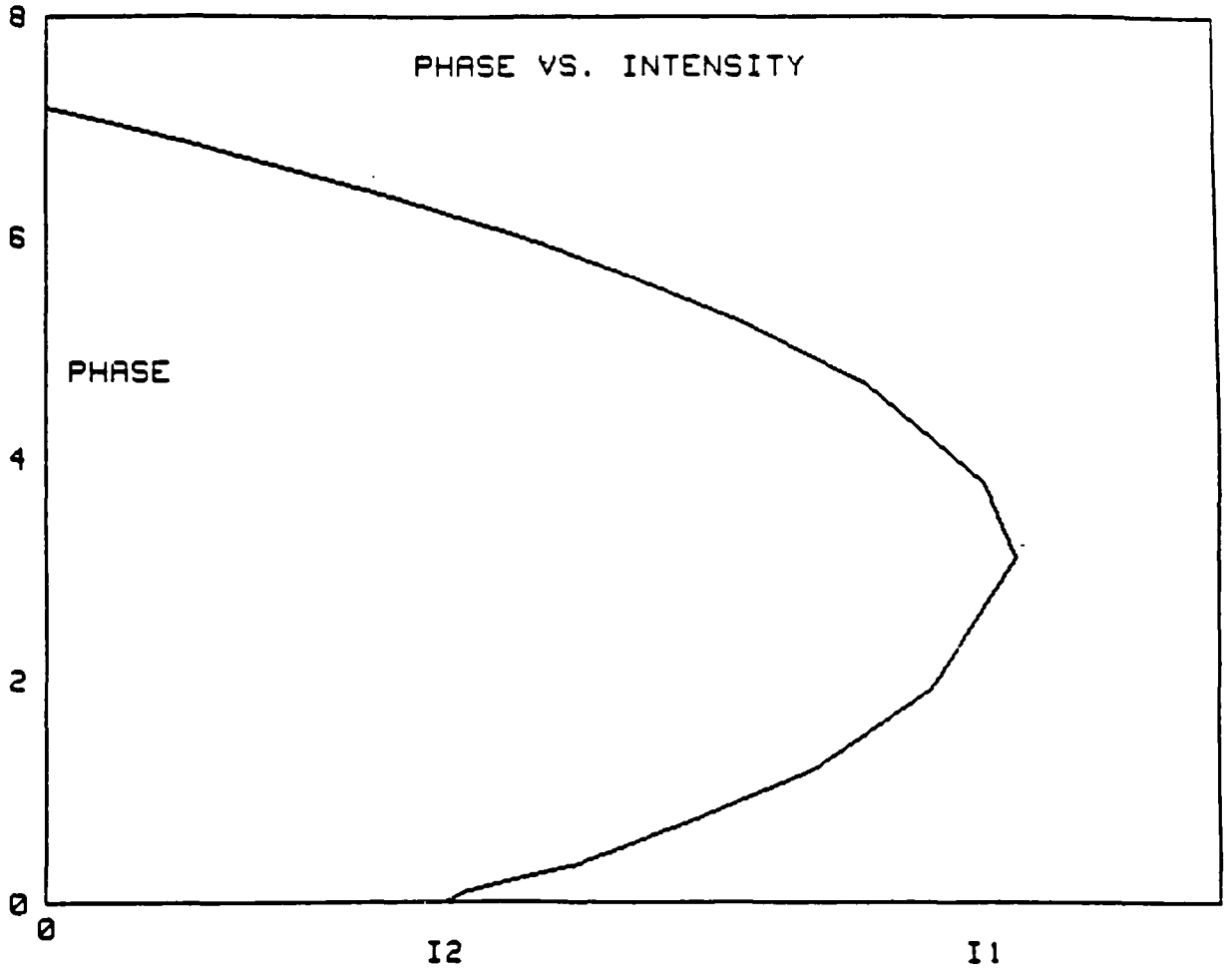

Fig. 5. Same as Fig. 4, but for $\theta = 7°$. (If $\theta < \theta_0 = \theta_c/\sqrt{2}(\approx .10°$ in the present case) both signs in (38) exist. The upper curve corresponds to the + sign, the lower one to the - sign in (38).)

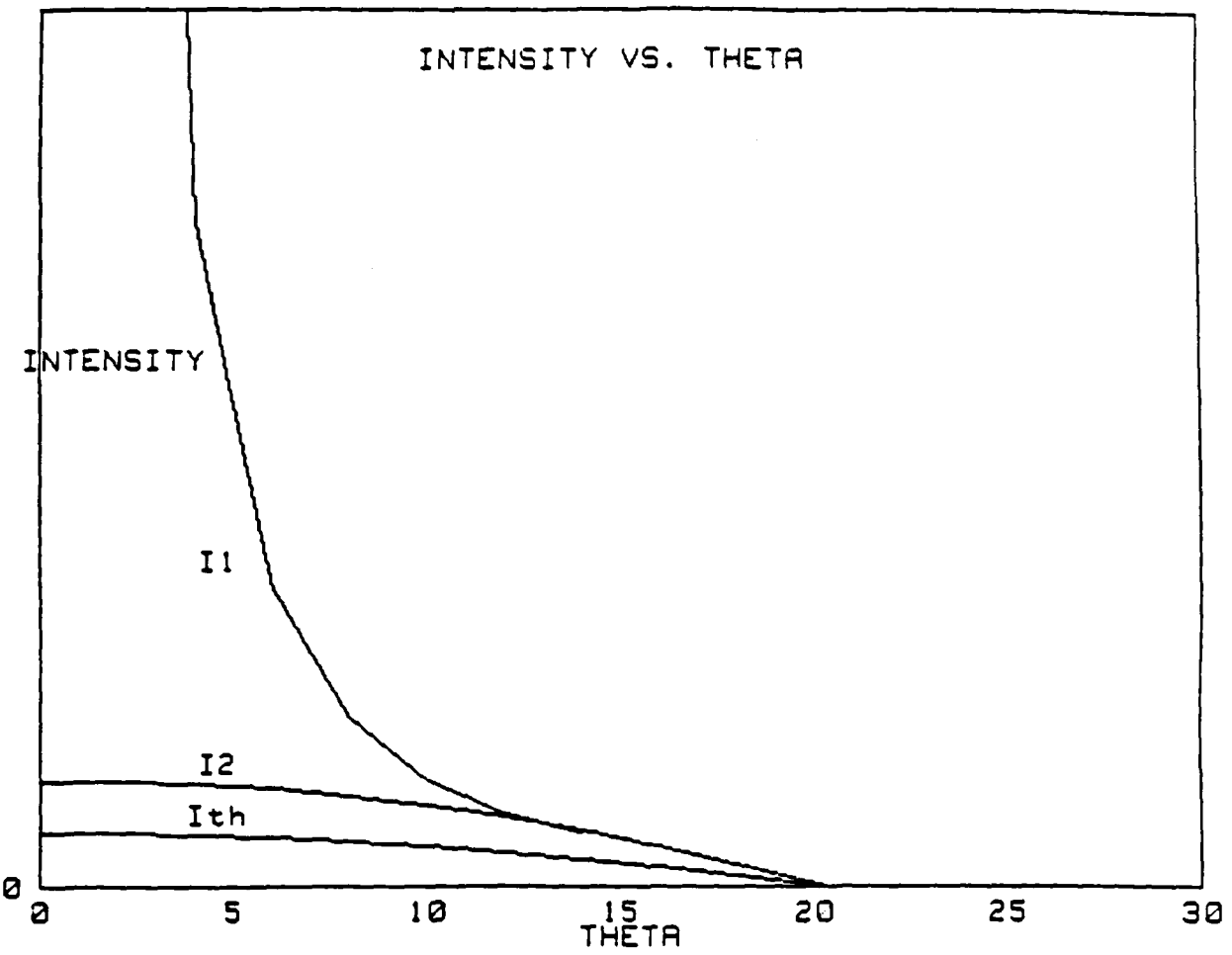

Fig. 6. Phase-plane of the reflection phenomenon from a nonlinear interface. (The reflection can be characterized by the angle of incidence θ and nonlinear intensity I. $I_{th}(\theta)$ is the threshold intensity, above which normal reflection exists. $I_1(\theta)$ is the limit intensity below which total reflection exits. $I_2(\theta)$ is the threshold intensity; for $I_2(\theta) < I < I_1(\theta)$ a second branch of the total reflection branch also exists. Since $I_{th}\theta < I_1(\theta)$ for $I_{th}(\theta) < I < I_1(\theta)$, the total reflection coexists with the normal reflection.)

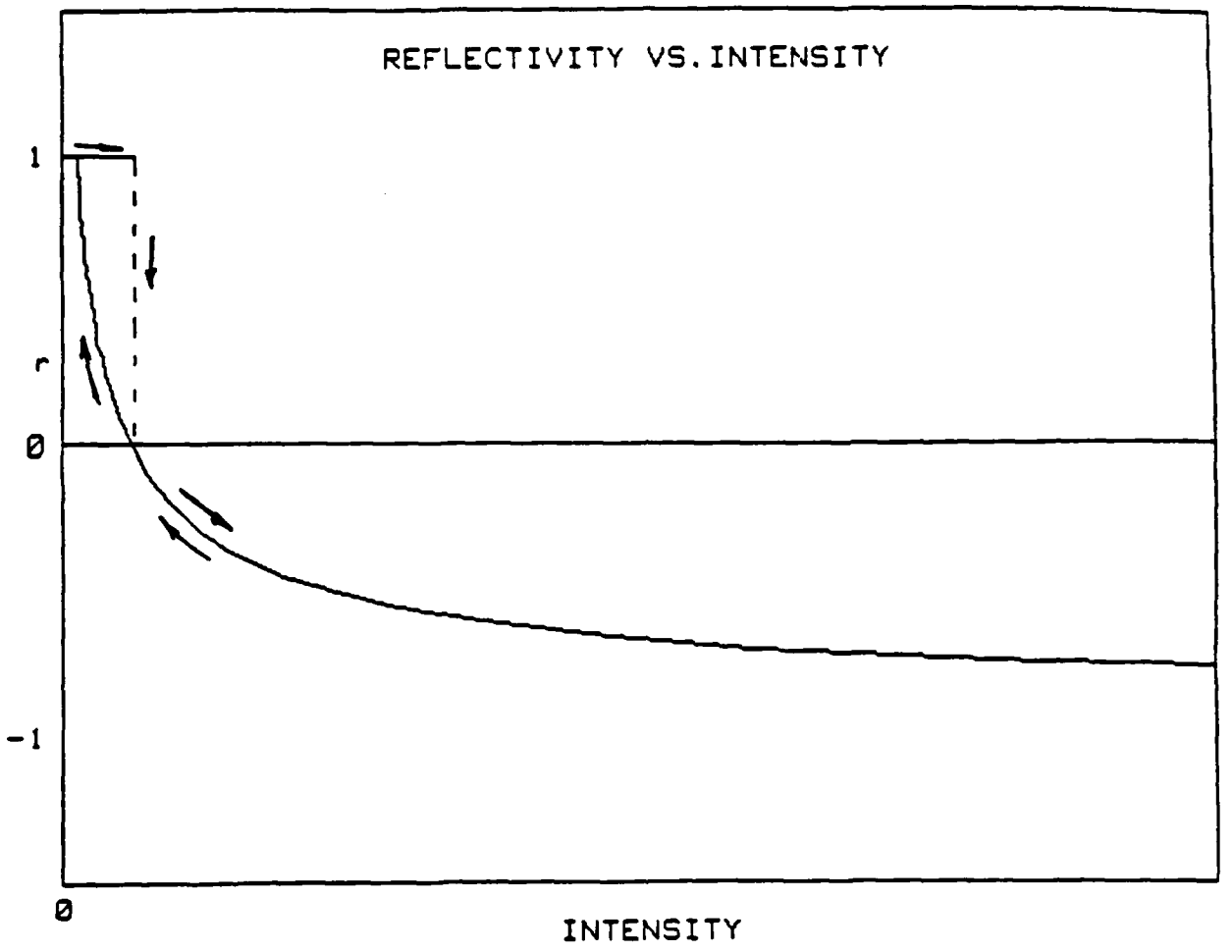

Fig. 7. Reflection r vs. nonlinear intensity I for total reflection and normal reflection in their region of coexistence. (The loop indicates the possibility of bistable behavior.)

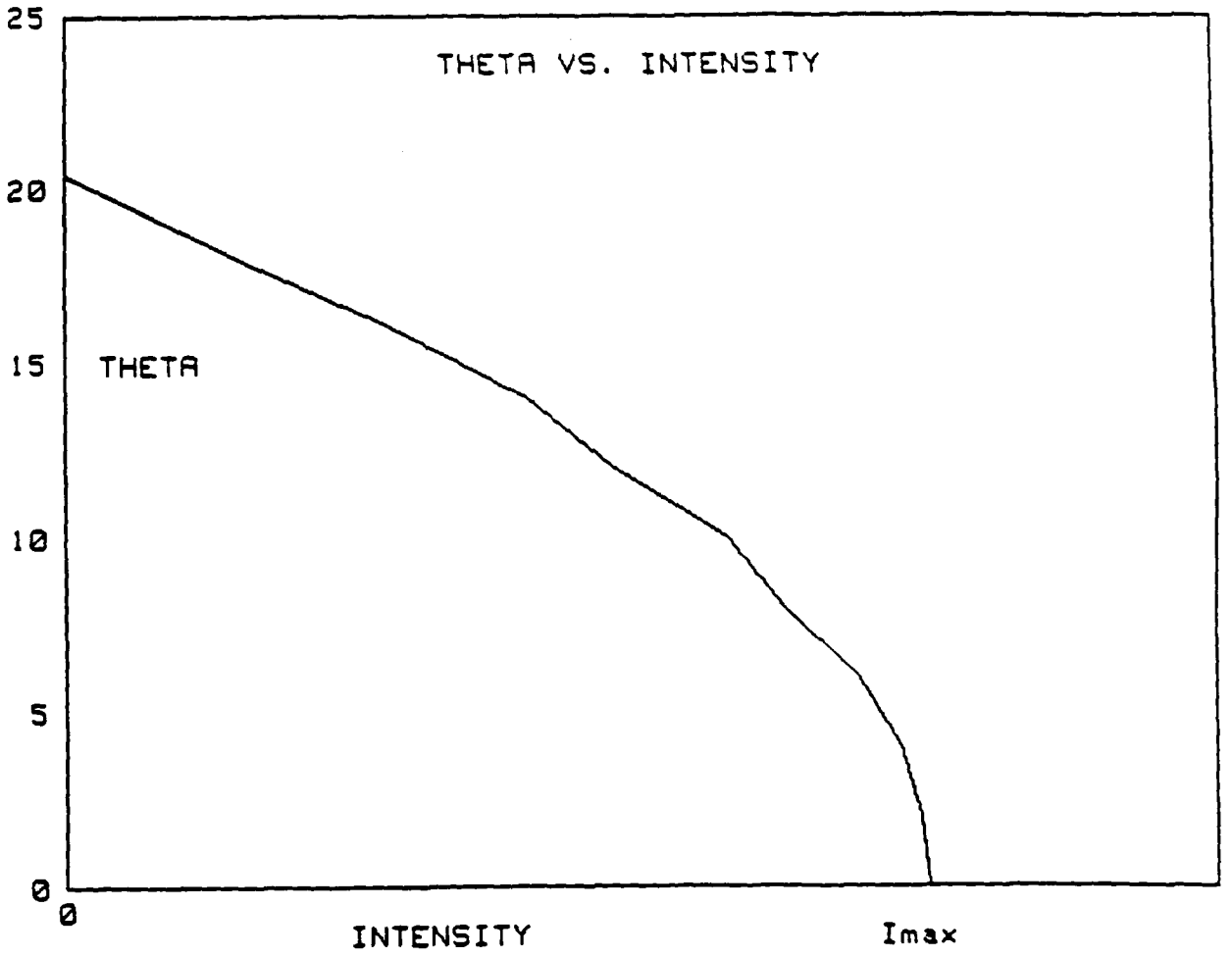

Fig. 8. Critical angle θ vs. nonlinear intensity I. (The plot corresponds to Eq. (30).)

3. ON THE INTRINSIC PROPERTIES OF NONLINEAR TE WAVES GUIDED BY A SYMMETRIC SLAB

3.1 INTRODUCTION

In recent years considerable theoretical effort has been devoted to the investigation of nonlinear optical waveguides. This interest is motivated by their capability to support soliton-type wave propagation and also to exhibit sudden switches between regimes with different guiding mechanisms. These features have a number of potential applications. Optical systems, in general, provide an accessible tool to study phase-transition-like phenomena occurring in nonequilibrium and/or nonlinear systems. A typical device is a resonator filled with a nonlinear medium (Ref. 1). In this case the transmission of the system becomes intensity dependent, because of the dependence of the effective optical length and absorption on intensity.

The purpose of this report is to analyze the optical wavequide bounded by nonlinear media as an alternative optical system having many of the described features. In previous works, attention was mainly focused on the problem of finding appropriate external (control) parameters and on the behavior of the system as these control parameters are varied. Although this is an important issue, from an experimental point of view, intrinsic features also have to be studied to achieve a full understanding of their behavior. Therefore, particular emphasis is placed here on revealing the mutual dependence of internal parameters which characterize a nonlinear guided wave propagating in the system. This enables us to determine the range of variation of the parameters, as well as to establish existence criteria for the various waves.

Historically, hysteresis reflection and refraction from a single nonlinear interface was first studied by Kaplan (Ref. 2). The evanescent wave solution given there was later successfully applied to the study of nonlinear surface polaritons (Refs. 3-4). After the initial proposals on optical bistability in nonlinear waveguides (Refs. 5-6), systems with two or more nonlinear interfaces were studied in detail on the basis of coupled mode theory (Ref. 7), which is valid only for weak nonlinearity. Application of exact methods to the nonlinear slab followed thereafter (Refs. 8-12). In an interesting paper Akhmediev predicted bistable switching between different branches of a given TE mode. Based on that work we elaborate the dependence on the propagation constant of various parameters appearing in the solution. We show, in particular, that this mutual dependence of various internal parameters suggests how these nonlinear waves can be excited, and determines the associated field patterns completely.

3.2 PARAMETER DEPENDENCE AND ASSOCIATED FIELD PATTERNS

Figure 9 shows the geometry of the problem under study. A slab with linear dielectric constant $\epsilon = \epsilon_1$ is embedded between two identical media with Kerr nonlinearity, $\epsilon = \epsilon_2 + \alpha|E(x)|^2$. For TE polarization E_y is the only nonvanishing component of the electric field. It is common to assume the form $E_y = E(x)\exp[i(\beta z - \omega t)]$, where β is the propagation constant.

Then the evanescent wave solution for guided modes in regions 2 and 3 can be written as (Ref. 8)

$$E(x) = \pm(2/\alpha)^{\frac{1}{2}}(\gamma/k)\sec h[\gamma(x - x_{2,3})]; \quad |x| > d \tag{43}$$

Here we assume $\alpha > 0$. We introduce the notation $\gamma^2 \equiv \beta^2 - k^2\epsilon_2$ and $k \equiv \omega/c$. γ is uniquely related to β. It is a constant associated with the propagation (attenuation) of evanescent waves along x. x_2 and x_3 are integration constants in regions 2 and 3, respectively.

The possible wave patterns in the linear region 1 are given by

$$E(x) = A\left\{\begin{array}{l} \cos[\kappa_1(x - d_0)]; A \\ \sin[\kappa_1(x - d_0)]; B \\ \cosh[\kappa_2(x - d_0)]; C; |x| < d \\ \sinh[\kappa_2(x - d_0)]; D \end{array}\right\} \tag{44}$$

Here $\kappa_1^2 \equiv k^2\epsilon_1 - \beta^2 > 0$ and $\kappa_2^2 \equiv \beta^2 - k^2\epsilon_1$. $\kappa_1(\kappa_2)$ is the constant associated with the propagation (attenuation) of guided waves along x in region 1 for $\kappa\sqrt{\epsilon_2} < \beta < k\sqrt{\epsilon_1}(k\sqrt{\epsilon_1} < \beta)$. A and d_0 are further constants of integration.

Boundary conditions require that $E(x)$ and $E'(x)$ be continuous at $x = \pm d$. This yields four relationships among the parameters in Equations 43 and 44. On the other hand, these field expressions contain five parameters: $A, x_2, x_3 d_0$, and β. This was not a problem in the linear case: due to linearity, A cancelled from the continuity equations and the remaining four parameters were determined completely (Ref. 13). In the linear

waveguide, in particular, $d_0 = 0$, i.e., all the field patterns are either completely symmetric or completely antisymmetric. Furthermore, $x_2 = -x_3 = -\infty$, so that evanescent waves are purely exponentially decaying ones. Also, β is restricted to certain discrete values (roots of the eigenvalue equations) in the interval $k\sqrt{\epsilon_2} < \beta < k\sqrt{\epsilon_1}$, so that no surface TE modes (hyperbolic patterns in 1) exist for $\beta > k\sqrt{\epsilon_1}$.

In the nonlinear case ($\alpha \neq 0$) the situation changes drastically. β becomes an interval continuous parameter; i.e., instead of assuming discrete values in the $k\sqrt{\epsilon_2} < \beta < k\sqrt{\epsilon_1}$ interval, as in the linear case, β can change continuously within discrete subintervals of the above interval. Also, values in the region $\beta > k\sqrt{\epsilon_1}$ (surface modes) become permissible. This can be seen from the following treatment. With the help of the four continuity equations we can express any of the other four parameters as a function of β. Each of these equations can, with equal rights, be regarded as a generalized eigenvalue equation of the nonlinear slab. They determine the physical domain of parameters, as well as the existence conditions for the different types of nonlinear waves (odd, even, asymmetric guided modes and surface modes).

For later convenience, and in order to bring the eigenvalue equations to their simplest form, it is useful at this point to introduce the scaled quantities $\tilde{x}_2 = x_2/d$, $\tilde{x}_3 = x_3/d$, $\tilde{d}_0 = d_0/d$. These dimensionless parameters determine the extremum positions of the field intensity distribution inside and outside the slab. We also introduce $a^2 = \frac{1}{2}\alpha A^2 k^2 d^2$, which is a nonlinear intensity parameter proportional to the intensity maximum in the slab. Instead of the propagation constant β we define two related parameters: $b_1^2 = (k^2\epsilon_1 - \beta^2)d^2$ for $\sqrt{\epsilon_2} < \beta < k\sqrt{\epsilon_1}$ and $b_2^2 = (\beta^2 - k^2\epsilon_1)d^2$ for $\beta > k\sqrt{\epsilon_1}$. Finally, we introduce the parameter $v^2 = (\epsilon_1 - \epsilon_2)k^2d^2$, which characterizes the waveguide itself. Once the waveguide is specified, v is fixed. The advantage of these scaled variables is that seemingly very different waveguides having the same parameter, v, exhibit similar behavior in terms of the scaled parameters. Thus, the usage of these parameters reveals universal properties of the nonlinear slab waveguide.

We now proceed to the investigation of the eigenvalue equations and the field patterns. We investigate the different possibilities enumerated in Equation 44 separately. Furthermore, we analyze in detail only the cases when the cos or cosh solutions hold in the slab. A complete treatment of all possible cases is left to a separate publication (Ref. 14).

3.2.1 We begin our investigation with the case when the first line holds in Equation 44. Then the boundary conditions allow for $\tilde{d}_0 = 0$ and $\tilde{d}_0 \neq 0$, as well.

3.2.1.1 If $\tilde{d}_0 = 0$, the field pattern is symmetric. In this case, from the boundary conditions we obtain

$$\tilde{x}_2 = -\tilde{x}_3 = 1 - (v^2 - b^2)^{-1/2} \tanh^{-1}[b_1 (v^2 - b_1^2)^{-1/2} \tan b_1] \tag{45}$$

which is our first eigenvalue equation.

Instead of a^2 we use the related parameter $S \equiv a^2 \cos^2 b_1$, which is the nonlinear intensity at the boundary. The other eigenvalue equation then reads as

$$S = v^2 - \frac{b_1^2}{\cos^2 b_1} \tag{46}$$

Equations 45 and 46, together with $\tilde{d}_0 = 0$, characterize the symmetric cosine wave completely, in the sense that the remaining parameters are expressed as functions of b_1 (i.e., the propagation constant β). Where in the interval $k\sqrt{\epsilon_2} < \beta < k\sqrt{\epsilon_1} (0 < b_1 < v)$ this wave may exist can be determined from the following argument. The criteria of existence are simply that $S > 0$ and that the argument of $\tanh^{-1}$ in Equation 45 should be between -l and l. Both these requirements lead to

$$b_1^2 \leq v^2 \cos^2 b_1 \tag{47}$$

i.e., such waves exist in those parts of the $0 < b_1 < v$ interval where Equation 47 holds. As expected, all solutions of Equation 47 lie in this interval. For any value of v there is always at least one such subinterval of b_1, i.e., the lowest order symmetric cosine mode never becomes cut off. As v increases, additional subintervals may appear. In these subintervals $\tilde{x}_2$ changes from $-\infty$ to ∞ as b_1 is changed from one boundary of the subinterval to the other. S is zero at the boundary of the subinterval, reaches a maximum inside and then falls back to zero again at the other boundary. It is interesting to note that at the right boundary of each subinterval the argument of $\tanh^{-1}$ in Equation 45 is equal to 1, so that

$$b_1 (v^2 - b_1^2)^{-1/2} \tan b_1 = 1 \tag{48}$$

This is just the eigenvalue equation for even TE modes of a linear waveguide. Also, at these points, $S = 0$. This suggests the following mechanism for the excitation of these nonlinear waves. At very small intensity S the system is essentially linear, and a guided

wave which is similar to a linear eigenmode can be launched. If we slowly increase S while allowing $b_1(\beta)$ to change according to Equation 46, then $\tilde{x}_2$ increases from $-\infty$ towards $+\infty$. At a threshold value of $S = S_1 (S_1 = v^2 - n^2\pi^2$ or $b_1 = n\pi$ for the n-th subinterval) we obtain $\tilde{x}_2 = 1$, and a real maximum of the field distribution outside the slab appears. At $S = S_{max} > S_1$ we reach the maximum of Equation 46, and S cannot be increased further along this branch of the dispersion curve. Thus, this mode becomes cut off at $S = S_{max}$ (or at $b_{1,max}$ corresponding to S_{max}, where $b_{1,max} = -\text{cotan}\, b_{1,max}$). The other side of this branch $b_1 < b_{1,max}$ cannot be reached with continuous excitation from the linear regime. It corresponds to two evanescent waves, excited initially infinitely far away from the slab boundaries. Increasing the intensity S at the boundary attracts these waves closer to the boundaries. Hence, they can only be excited under conditions very different from those of a waveguide. Figure 10 shows the dispersion relation (plot of Equation 46) for $v = \frac{3}{2}\pi$. In this case TE_0 and TE_2 modes are allowed. Also shown are two typical TE_2 field patterns for $S < S_1$ and $S_1 < S < S_{max}$. The guiding mechanism for $S > S_1$ is obviously different from the usual total internal reflection (TIR) of linear waveguides. It can adequately be described as self-focusing in the nonlinear medium.

This is not the whole story, however. The effective refractive indexes on the two sides of the slab boundary become equal if the intensity satisfies $\epsilon_1 = \epsilon_2 + \alpha|E(d)|^2$ or, in our notation, $S = \frac{v^2}{2}$. At this intensity the boundary becomes transparent, and we might expect something strange to happen. That this is indeed the case is made clear in the next subsection.

3.2.1.2 Here we investigate the $\tilde{d}_0 \neq 0$ case, where the field pattern is asymmetric. The analytic expression for $\tilde{d}_0$, resulting from the continuity equations, is

$$\sin^2 b_1 \tilde{d}_0 = \left(1 - \frac{b_1^2}{v^2}\right) r + \frac{b_1^2}{v^2}(1 - r) - \left(4r(l - r)\frac{b_1^2}{v^2}\left(1 - \frac{b_1^2}{v^2}\right) + \frac{b_1^4}{v^4}\right)^{1/2} \tag{49}$$

Here $r = \cos^2 b_1$. In this case $\tilde{x}_t \neq -\tilde{x}_3$, and these quantities are given by

$$\tilde{x}_{2,3} = \pm 1 \mp (v^2 - b_1^2)^{-1/2} \tanh^{-1}\left\{b_1 (v^2 - b_1^2)^{-1/2} \tan\left[b_1 (1 \mp \tilde{d}_0)\right]\right\} \tag{50}$$

The nonlinear intensities at the boundaries $\pm d$, $S =_{\pm} = a^2[b_1(1\pm \tilde{d}_0)]$, can be written in the more symmetric form

$$S_{\pm} = \frac{v^2}{2} \pm \frac{b_1^2}{2}\left\{\frac{1}{\cos^2[b_1(1-\tilde{d}_0)]} - \frac{1}{\cos^2[b_1(1+\tilde{d}_0)]}\right\} \tag{51}$$

The criterion of existence of these asymmetric guided waves is that $0 \leq \sin^2 b_1 \tilde{d}_0 \leq 1$, or the argument of $\tanh^{-1}$ in Equation 50 should be between -1 and 1, or $S\pm \geq 0$. All these requirements lead to

$$b_1^2 \leq \frac{v^2}{2}\cos^2 b_1 \tag{52}$$

i.e., such waves exist in those parts of the $0 \leq b_1 \leq v\sqrt{2}\left(k\frac{\sqrt{\epsilon_1+\epsilon_2}}{2} < \beta < k\sqrt{\epsilon_1}\right)$ interval where Equation 52 holds. For any value of v there is always at least one such subinterval of b_1, i.e., the lowest order asymmetric mode never becomes cut off. As v increases, additional subintervals may appear. In these subintervals, $\tilde{d}_0$ changes such that $0 \leq b_1 \tilde{d}_0 < \pi/2$, and it is 0 at both boundaries of the subinterval. The boundaries of these subintervals are defined by the equality sign in Equation 52. The nonlinear intensity at these points is $S_+ = S_1 \equiv S_{th} = v^2/2$, as can be seen from Equation 51. Thus, the asymmetric waves branch away from the symmetric ones at the intensity which makes the boundary transparent. Consequently, their appearance is a threshold phenomenon.

In Fig. 11 we have plotted the dispersion relation, Equation 51, and two typical asymmetric field patterns developing from the symmetric TE_2 mode for $S > S_{th}$. In that part of the b_1 interval where the symmetric and asymmetric waves coexist, the asymmetric one carries less energy. This may indicate that the asymmetric wave is generally more stable and that the part of the dispersion curve of the symmetric modes above S_{th} is difficult to reach.

This dispersion curve together with the dispersion curve of the symmetric TE_2 mode of Fig. 10 hints at the following interesting possibility. If the intensity at the boundary is increased along S_+, then at $S_{m,1}$ we reach the maximum of the S_+ branch. Denote the corresponding b_1 value by $b_{1,m}^{(1)}$. If we try to increase the intensity further, the system may jump over to the S_- branch, along which the intensity can be increased up to

the value $S_{m,2}$. At this value this type of asymmetric mode becomes cut off. If we lower the intensity along the S_- branch we reach the minimum at a point where $b_1 = b_{1,m}^{(1)}$. This is the same value where the $S_+ \rightarrow S_-$ jump occurs, but with the role of the upper and lower boundaries interchanged. The system at this point may jump over to the symmetric TE_2 branch of Fig. 10. (Actually, these two figures should be viewed together. Only for clarity are they represented separately.) If now the intensity is increased along this branch, we eventually reach S_{th}. Further increase of the intensity excites the S_+ branch of the dispersion curve. The excitation loop completed this way would then contain bistable jumps with hysteresis. Since the asymmetric waves carry less power than the symmetric ones, lowering the intensity along S_- requires less input power than increasing it along TE_2. This is in good qualitative agreement with the experimental observation of Ref. 15. It is also clear that this type of bistability cannot occur in the lowest order mode, since S_+ and S_- branching away from TE_0 (the left portion of Fig. 11) do not exhibit this structure. This conclusion is also supported by the experiment.

3.2.2 Except that the v dependence plays a more important role, the antisymmetric sine wave obtained when the second line holds in Equation 44 has similar properties to the ones discussed above. Therefore, we do not elaborate further on this case. A complete discussion is given in Ref. 14.

3.2.3 We next investigate the case when the third line holds in Equation 44, the case of the cosh wave. Since the boundary conditions now allow $\tilde{d}_0 = 0$ only, the wave is completely symmetric. The analytic expressions for the other parameters are

$$\tilde{x}_2 = -\tilde{x}_3 + 1 + \left(b_2^2 + v^2\right)^{-1/2} \tanh^{-1}\left[b_2 \left(b_2^2 + v^2\right)^{-1/2} \tanh b_2\right] \tag{53}$$

For the nonlinear intensity at the boundary, $S = a^2 \cosh^2 b_2$, we have

$$S = v^2 + \frac{b_2^2}{\cosh^2 b^2} \tag{54}$$

The criterion of existence is $S > v^2$, or the argument of $\tanh^{-1}$ in Equation 53 should be less than 1, which is fulfilled in the entire $b_2 > 0 (\beta > k\sqrt{\epsilon_1})$ interval for all v. The intensity for $b_2 = 0$ $(\beta = k\sqrt{\epsilon_1})$ is v^2, and this value coincides with the intensity of the lowest order symmetric cosine mode at $b_1 = 0$ $(\beta = k\sqrt{\epsilon_1})$. This suggests that the symmetric surface modes described by the hyperbolic cosh solution can be reached by increasing

the intensity of the lowest order symmetric cosine mode and tuning from $\beta < k\sqrt{\epsilon_1}$ to $\beta > k\sqrt{\epsilon_1}$. The appearance of the surface mode is a threshold phenomenon requiring the minimum nonlinear intensity $S_{th} = v^2$. Figure 12 shows a plot of the dispersion relation, Equation 54, and a typical field pattern. If b_2 is increased, S increases first, reaches a maximum $S = S_{max}$ at a certain $b_2 = b_{2,max}$, and then decreases monotonically. Obviously, only that part of the dispersion curve for which $S < S_{max}$ can be reached by continuous excitation from the $\beta < k\sqrt{\epsilon_1}$ regime. At this point this surface mode becomes cut off. The decreasing part corresponds to a very different excitation condition: surface modes are excited outside the slab. It is interesting to observe the behavior of $\tilde{x}_2$ as a function of b_2. As b_2 is increased, $\tilde{x}_2$ increases first, starting from the value 1 at $b_2 = 0$, reaches a maximum at $b_2 = b_{2,max}$ and decreases again towards $\tilde{x}_2 = 2$ as $b_2 \to \infty$. That is, the position of the maximum of the field distribution always remains in the vicinity of the slab boundary, justifying the name "surface mode."

3.2.4 The case when the fourth line holds in Equation 44 (hyperbolic sine wave) is discussed in Ref. 14.

3.3 CONCLUSION

The symmetric slab waveguide bounded by nonlinear media can support symmetric, antisymmetric and asymmetric guided waves and surface modes. The latter two have no counterpart in the linear case. Their appearance is a threshold phenomenon: a threshold intensity at the slab boundary is needed for their excitation. By appropriate scaling of the parameters characterizing the different waves, we cast the dispersion relations of these waves into particularly simple form. This enables us to establish existence conditions for various types of waves and to determine the range of variation of all the parameters involved. Also, the interpretation of the results is facilitated. For example, the threshold intensity for the appearance of asymmetric waves is the intensity which makes the boundary transparent. The threshold intensity for the appearance of a surface mode is the intensity where the lowest order guided mode terminates. The dispersion relations in this scaled form are also very suggestive as to the excitation of these waves. At very small values of the nonlinear intensity at the boundary, the dispersion relations reduce to the eigenvalue equations of a linear waveguide. It is known how an eigenmode of a linear waveguide can be launched. Upon increasing the nonlinear intensity adiabatically, one can consecutively excite different portions of that branch of the dispersion relation which originates from a given linear limit. Furthermore, our results seem to indicate the possibility of a bistable loop in the excitation process of higher order modes in qualitative accord with recent experimental findings.

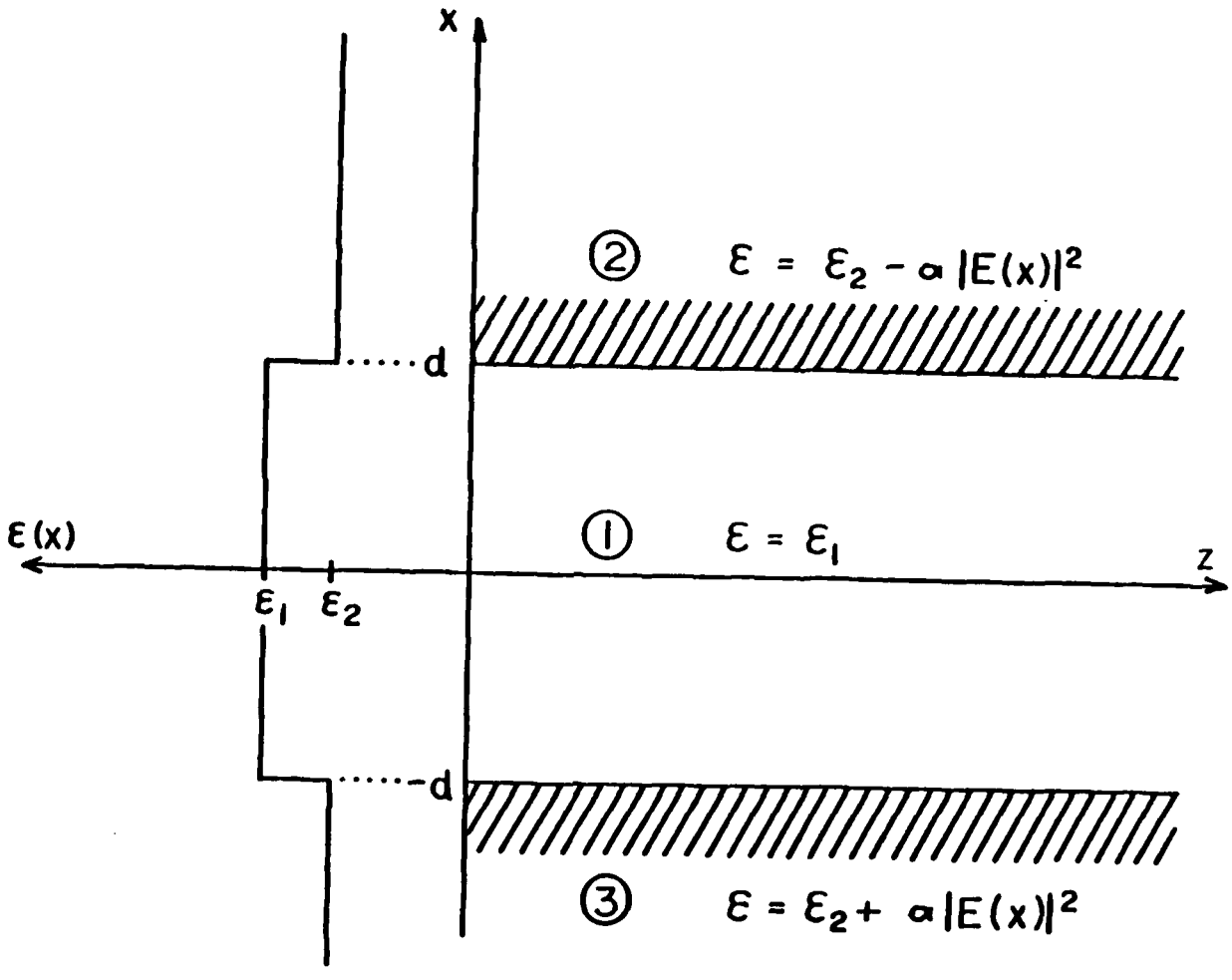

Fig. 9. Geometry of the slab configuration.

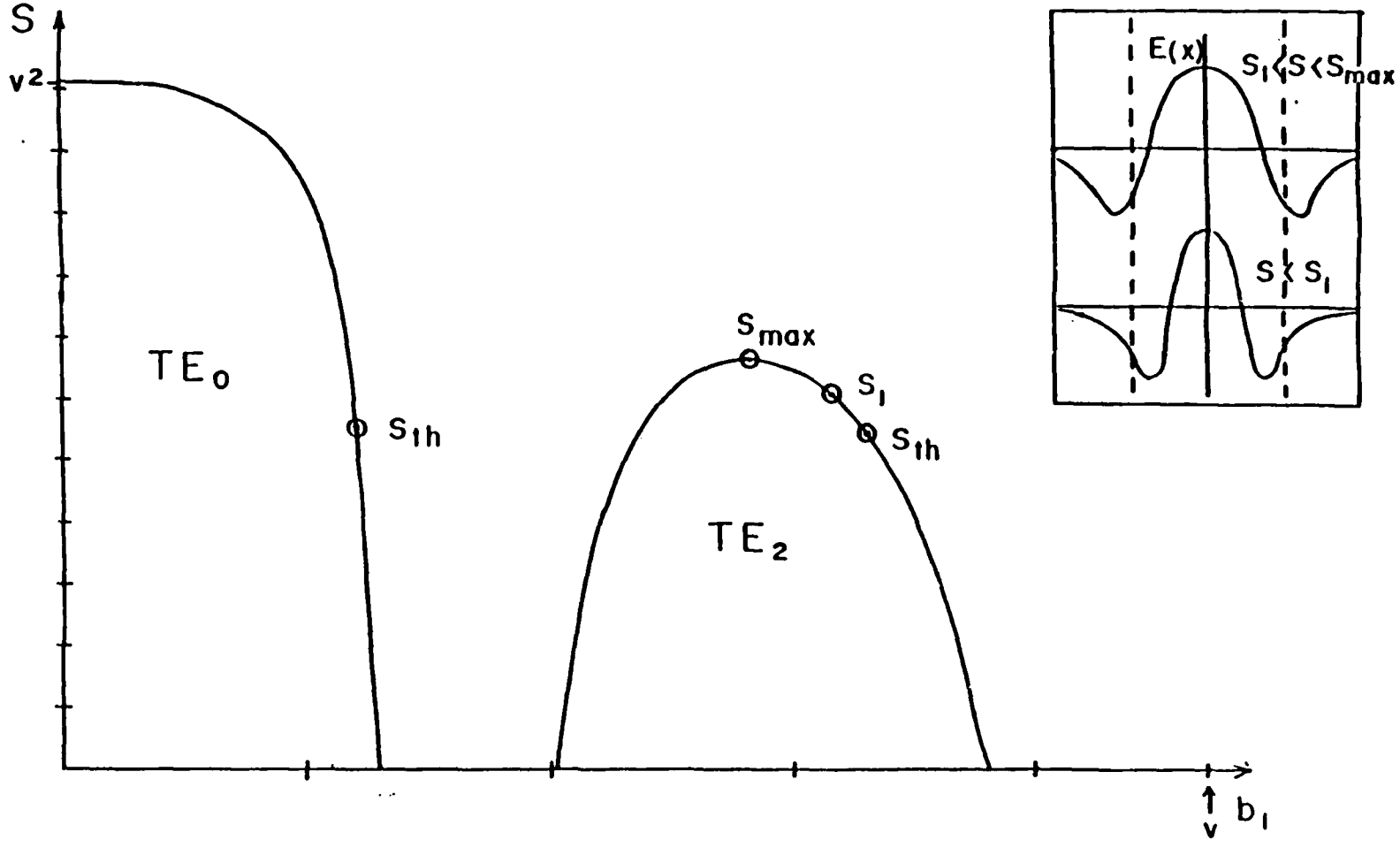

Fig. 10. Dispersion curve (intensity at the slab boundary vs. propagation constant) for the symmetric cosine modes and for v = 5. (Also shown are field patterns belonging to the $S_1 < S$ and $S_{max} > S$ portion of the TE branch of the dispersion curve.)

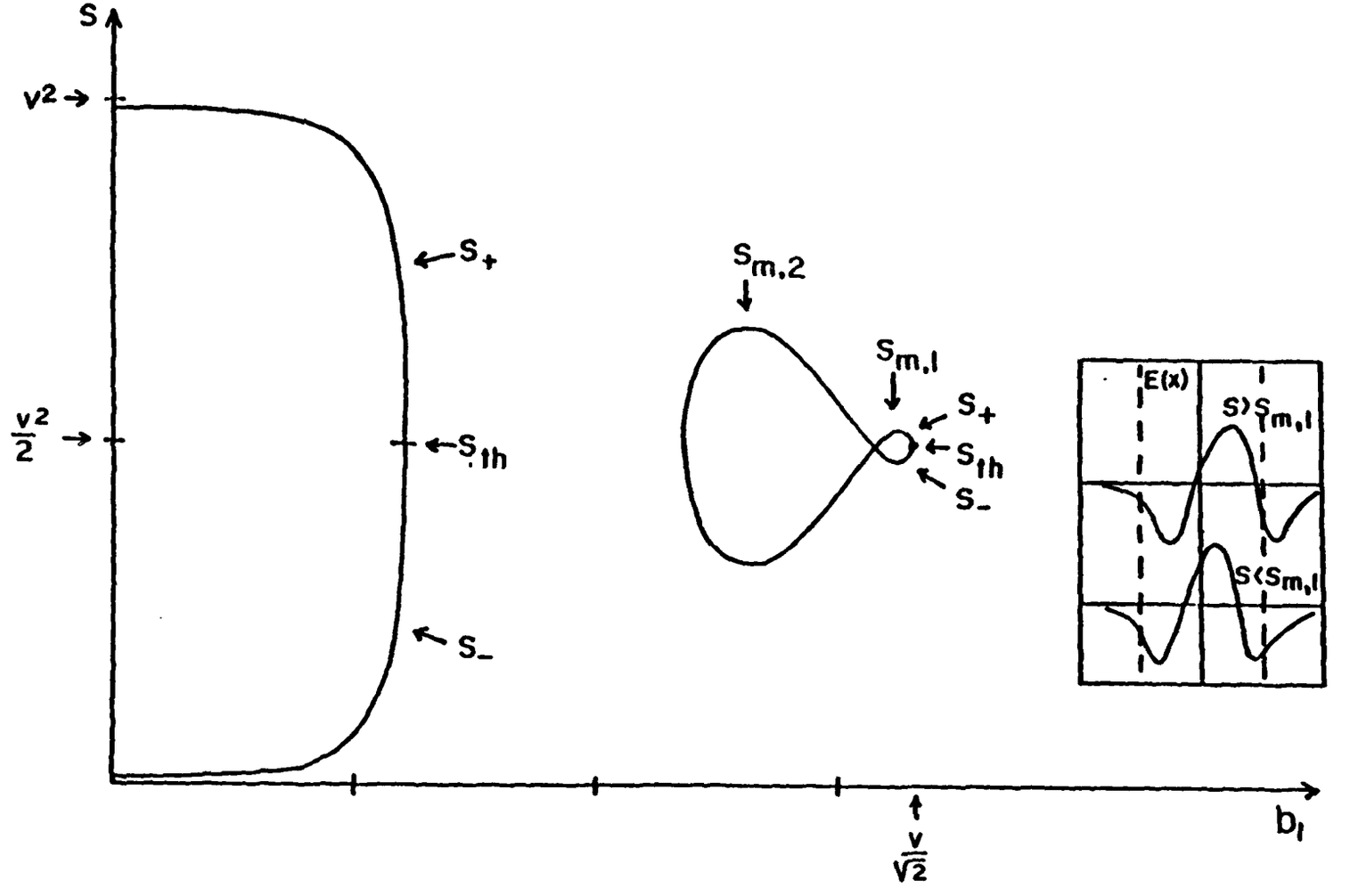

Fig. 11. Dispersion curve and field pattern of the asymmetric cosine wave.

Fig. 12. Dispersion curve and field pattern of the symmetric hyperbolic cosine surface mode.

4. INTENSITY DEPENDENCE OF TOTAL VERSUS DIFFERENTIAL IONIZATION RATES IN ABOVE-THRESHOLD IONIZATION (REF. 16)

In above-threshold ionization, total ion yields conform with lowest order perturbation theory up to much higher intensities than the individual peaks of the electron spectrum. This fact is explained and an estimate of the intensity is derived for which the total ionization rate ceases to follow lowest order perturbation theory. The derivation uses arguments based on simple dimensional analysis.

Multiphoton ionization of atoms by intense laser fields has been investigated for many years (Ref. 1). In all cases, for intensities up to about $10^{15} W/cm^2$, the total ionization rates below saturation as measured via the total ion yields were found to be proportional to the Nth power of the laser intensity I, with N the minimum number of laser photons which the atom has to absorb to be ionized. This I^N - behavior is readily explained on the basis of lowest order perturbation theory with respect to the laser field. On the other hand, the more recent experiments recording the energy spectra of the ejected electrons start revealing markedly nonperturbative features for intensities as low as $10^{13} W/cm^2$ (Refs. 17-22). A typical ATI (above-threshold ionization) electron spectrum exhibits equally spaced peaks, separated by the energy $\hbar\omega$ of a laser photon, at energies

$$\mathcal{E}_N = \mathcal{E}_0 + n\hbar\omega \qquad (n = 0, 1, 2...) \tag{55}$$

While perturbation theory suggests that the height of the n^{th} peak be proportional to I^{N+n}, experiments show that for intensities $\gtrsim$ *im* $10^{13} W/cm^2$ this is no longer so: the lowest peak ($n = 0$) is no longer the dominant one (peak switching); moreover, the low-order peaks become, for increasing intensities, one at a time completely suppressed (peak suppression). The heights of the individual peaks approximately scale with $I^{N-\frac{1}{2}}$ (Ref. 17) for most n (the lowest peak with a power less than this) rather then with I^{N+n}. Deng and Eberly (Ref. 23) identified an intensity $I_{sat} \sim 10^{12} W/cm^2$ such that for $I \gtrsim I_{sat}$ lowest order perturbation theory ceases to be valid for the individual peaks. At the same time, it still holds perfectly well for the total ionization rates (Ref. 24). The same behavior has also been observed in numerical analyses (Ref. 25). It is the purpose in this report to make this apparent puzzle plausible and to identify an intensity $\bar{I}_{sat} >> I_{sat}$ so that for $I \gtrsim \bar{I}_{sat}$ lowest order perturbation theory (LOPT) becomes inapplicable for the total rate. We will proceed on the basis of simple dimensional analysis without assuming any specific model.

We first notice that the behavior just described appears to be a quite common phenomenon in multiphoton physics. We may summarize it by stating that often the total transition rate for some process in the presence of a laser field can be calculated by perturbation theory for much higher intensities than the corresponding differential transition rates. For example, for the case of the free-electron laser, the probability p_n that the electron emits n laser photons while it travels through the undulator is a very complicated function of the laser intensity and only calculable by LOPT for extremely low intensities. On the other hand, the gain, which is proportional to $\sum_{n=-\infty}^{\infty} np_n$, can be obtained from LOPT up to intensities which are higher by about eight orders of magnitude (Ref. 26). Another well-known example is the Kroll-Watson sum rule for electron-potential scattering in the presence of a laser field, which says that under certain conditions the total cross section $\sigma = \sum_{n=-\infty}^{\infty} \sigma_n$ (σ_n being the cross section with accompanying emission of n laser photons) just equals the cross section σ_{free} in the absence of the laser field (Ref. 27). In this case LOPT obviously yields $\sigma = \sigma_{free}$ while it is not applicable for the σ_n.

Before returning to ATI we shall extensively consider laser enhancement of nuclear β-decay as an additional example. This is a particularly convenient case because the decay rate has been evaluated, and LOPT has been proven to hold. The very simple result for the field-induced enhancement of the decay is (Ref. 28)

$$\rho \equiv \frac{\Gamma_{field} - \Gamma_0}{\Gamma_0} = k\left(\frac{E}{E_c}\right)^2\left(\frac{mc^2}{\epsilon_0}\right)^3 = k\frac{(eE)^2\hbar^2}{m\epsilon_0^3} \tag{56}$$

for $E < E_c$ and $\epsilon_0 \ll mc^2$. Here E is the field strength of the (circularly polarized) laser field, $E_c = m^2c^3/e\hbar \sim 1.6 \times 10^{16} V/cm$ the so-called critical field, m the electron mass and ϵ_0 the nuclear energy release of the decay minus the electron's rest mass energy. The quantity k is a numerical factor (k = 35/64 for allowed β-decay, and k = 105/32 for a first-order forbidden decay). In contrast to the simple form (Eq. 56) of the enhancement of the total rate, the differential decay rate with respect to the energy E_β of the emitted electron, viz., $d\Gamma_{field}/dE_\beta$, has a very complicated dependence on the field strength (Ref. 29) and cannot be obtained from perturbation theory except when E/E_c is extremely small.

We will now try to rederive Equation 56 from dimensional considerations. Let us first list the relevant variables: besides $m, c, \hbar$, and e, there is the field strength E and frequency ω of the laser field, the nuclear energy release ϵ_0 and the extent R of the nuclear

wave function. A complete set of dimensionless quantities that can be formed out of these is given by $E/E_e, \epsilon_0/mc^2, \sqrt{m\epsilon_0}R/\hbar, \alpha = e^2/\hbar c$, and $eE/m\omega c$. We now make the following assumptions or observations:

(a) A glance at the form of the matrix element that has to be calculated to obtain the exact result (Eq. 56) makes clear (Ref. 28) that the enhancement will depend on even powers of eE and that this is the only occurrence of the charge e. There is then no additional dependence on $\alpha = e^2/\hbar c$;

(b) the enhancement is a quantum effect, so that we should have $\rho \to 0$ for $\hbar \to 0$;

(c) since normally $\epsilon_0/mc^2 << 1$, and $\hbar\omega/mc^2 << 1$, the leading contribution to ρ is nonrelativistic, i.e., independent of c;

(d) the dynamics are quasistatic, i.e., the enhancement depends only on the field strength E and not explicitly on the frequency ω of the laser field.

By assumption (d), any dependence of ρ on the vector potential $a = eE/\omega$ or on the dimensionless parameter $eE/m\omega c$ is ruled out. This leaves us with the three dimensionless quantities $E/E_e, \epsilon_0/mc^2, \sqrt{m\epsilon_0}R/\hbar$ to build the dimensionless enhancement ρ. Observation (a) forces the leading contribution to ρ to be proportional to $(E/E_e)^2$, (c) then makes necessary the factor of $(mc^2/\epsilon_0)^3$ in order to cancel the dependence on c. This yields the result (Eq. 56) which satisfies assumption (b). The latter would still be satisfied with an additional factor of $\sqrt{m\epsilon_0}R/\hbar$; however, $\sqrt{m\epsilon_0}R/\hbar \sim 0(10^{-3})$, so this would not be the leading contribution. Assumption (b) is also satisfied when the r.h.s. of Equation 56 is multiplied by arbitrary inverse powers of $\sqrt{m\epsilon_0}R/\hbar$. However, the enhancement ρ would then become proportional to inverse powers of the nuclear radius R. This is highly implausible in view of the fact that the matter-field coupling can be taken as $\vec{r} \cdot \vec{E}$. We thus see that the assumptions (a) to (d) essentially prescribe the form (Eq. 56) for the leading contribution to the enhancement. Moreover, assumption (a) is really an observation. The same applies to assumption (b), although in a less obvious way: if one describes the β-decay by the quartic Fermi-interaction, then the laser field couples to the charged particles taking part in the process, notably the electron. This has two effects: first, a classical acceleration of the electron after the decay has taken place. This distorts the differential decay rate, but leaves the total rate unaffected; second, the decay rate itself is altered. This comes from off-shell contributions of the electron propagator adjacent to the four-Fermi-vertex. Hence, any enhancement of the decay must be quantum mechanical and proportional to some positive power of $\hbar$. Assumption (c) is justified by noticing that relativistic corrections would have to involve positive powers of the quantity ϵ_0/mc^2, which is small for the small nuclear energy releases we are considering. (For $\epsilon_0/mc^2 \lesssim 1$, assumption (c) and Equation 56 do not hold.)

The quasistatic assumption (d) is crucial for the above analysis. It is highly plausible for nuclear β-decay, which proceeds on a time scale much faster than the time scale ω^{-1} of the laser field and on a spatial scale much smaller than the laser wavelength. The dimensionless quantity $ea/mc^2 = eE/m\omega c$ (the occurrence of which in the total decay rate is ruled out by assumption (d)) plays, however, the dominant role in the interaction between the electron and the laser field after the decay and, consequently, in the differential decay rate. This is obvious by noticing that the solution of the nonrelativistic equation of motion $m\ddot{x} = eE\sin\omega t$ is $v/c = -(eE/m\omega c)\cos\omega t + const.$ Hence the parameter $eE/m\omega c$ governs the large-scale motion of the electron in the laser field (which is of the order of the wavelength).

We now apply the same reasoning to above-threshold ionization. For low enough intensities the ionization rate per unit time allows for a power series expansion in terms of the intensity I

$$\Gamma = \sum_{n=0}^{\infty} \Gamma_n = \Gamma_0 (1 + \sum_{n=1}^{\infty} \Gamma_n / \Gamma_0) \tag{57}$$

where $\Gamma_n \sim I^{N+n}$, with N as defined above. The question then, which we shall try to answer, is for which intensity I_{sat} the leading correction Γ_1/Γ_0 to the I^N-behavior will become important. (For the individual peaks this intensity is given by I_{sat}.) The problem is almost analogous to field-enhanced β-decay. The most notable difference is that β-decay takes place also in the absence of the field, whereas in ATI $\Gamma_0 \sim I^N$. If we describe the atom by just a radius R and an ionization potential V (replacing ϵ_0) the list of parameters is the same as above, although some of their values are different. Consequently, the set of dimensionless quantities is the same. We again make the assumptions (a) to (d). Assumption (a), provable by inspection in the case of β-decay, will hold for ATI as long as no additional energy or length scales enter the problem, so that all occurrences of the elementary charge which are of atomic origin are hidden in the constants R and V. This will not be so if there are near-resonant intermediate states. Even then, however, these may well predominantly affect Γ_0 and much less so the ratio Γ_1/Γ_0. Assumption (b) appears to be debatable since, after all, ionization can follow completely classical, chaotic routes (see, e.g., Ref. 30). However, we will see below that this hardly affects our estimate (as long as we do not expand our list of relevant parameters). There is no problem with assumption (c). Assumption (d) is less well satisfied for ATI than for β-decay, but should still be safe, since the atomic length scale is much smaller than the laser wavelength.

It is then obvious that we obtain the same result as before for the leading correction to the total ionization rate, viz.,

$$\frac{\Gamma_1}{\Gamma_0} = k' \frac{(eE)^2 \hbar^2}{mV^3} \tag{58}$$

with a different undetermined constant k'. Assuming $0(k') = 1$, we have $0(\Gamma_1/\Gamma_0) = 1$ for

$$(\frac{E}{E_B})^2 \equiv \frac{\bar{I}_{sat}}{I_B} \sim \left(\frac{V}{mc^2}\right)^3 \left(\frac{\hbar c}{e^2}\right)^6 = \left(\frac{V}{mc^2\alpha}\right)^3 \tag{59}$$

where $E_B = e/a_0^2 (a_0 = \hbar^2/me^2)$ is the Bohr field and $I_B = cE_B^2/4\pi = 7.1 \times 10^{16} W/cm^2$ the corresponding intensity. For $V \sim 10eV$ this yields $\bar{I}_{sat} \sim 5 \times 10^{-2} I_B \sim 10^{15} W/cm^2$. This defines the intensity $\bar{I}_{sat} >> I_{sat}$ mentioned in the Introduction. Equation 59 is the main result of this section. It explains the observed persistence of the I^N behavior of the total ionization rate, as opposed to the nonperturbative behavior of the ionization rate into individual peaks, and predicts an order of magnitude for the intensity for which corrections will become important.

Assumption (b) could be relaxed to allow for Γ_1/Γ_0 to be independent of $\hbar$ or even proportional to negative powers of $\hbar$ as long as Γ_1 is proportional to a positive power. The r.h.s. of Equation 58 would then be multiplied with some power of the dimensionless quantity $\sqrt{mV}R/\hbar$. However, for $V = 10eV$ and $R = 10^{-8} cm$ we have $\sqrt{mV}R/\hbar = 1.15$, so that the order of magnitude of Γ_1/Γ_0 is unchanged. If Γ_1/Γ_0 is considered to be related to an $(N+1)$ - quantum process, the expression given in Equation 58 seems to be the more logical one. It can readily be checked that the leading relativistic corrections to Γ_1/Γ_0 are very small.

It should be emphasized again that our assumption (d) implies that the total ionization rate is independent of the quantity $eE/m\omega c = ea/mc^2$. This latter quantity characterizes the ponderomotive potential, which has a very significant impact on the ATI electron spectrum for intensities $I \gtrsim I_{sat}$ (Ref. 31). Since, however, the former is related to the large-scale quivering motion of an electron in a laser field, it should play no role in the total ionization rate. Hence, even when many of the low energy peaks of the electron spectrum are already suppressed, the total rate still is proportional to I^N. For intensities up to $10^{15} W/cm^2$, this has been experimentally observed in some cases (Ref. 24). As has been remarked by Lompré et al. (Ref. 22), it may therefore be misleading to think of the ponderomotive potential as added to the ionization potential.

Of course, the predictive power of a result derived by dimensional arguments is limited. Should the experimental value for $\bar{I}_{\ldots}$ turn out to be in major disagreement with Equation (59), this could be due to (1) a value of the numerical factor k' significantly different from unity, (2) more parameters than assumed above playing a decisive role or (3) any of the assumptions (a) to (d) being violated. Any of these findings would be of interest by themselves. In any event, since an experimental value is presently not known, Equation 59 gives an estimate of where one might expect deviations from the I^N behavior.

REFERENCES

1. E. Abraham and S. D. Smith, Rep. Prog. Phys. **45** (1982) 815.
2. A. E. Kaplan, Sov. Phys. JETP **45** (1977) 896.
3. V. M. Agranovich, V. S. Babichenko, and V. Ya. Chernyak, JETP Lett. **32** (1980) 512.
4. W. J. Tomlinson, Optics Lett. **5** (1980) 323.
5. P. W. Smith, W. J. Tomlinson, and P. T. Maloney, J. Opt. Soc. Am. **70** (1980) 658.
6. A. E. Kaplan in 'Optical Bistability' ed. M. Bowden (Plenum, N. Y., 1981) p. 447.
7. G. I. Stegeman, IEEE MTT-30 (1982) 1598.
8. N. N. Akhmediev, Sov. Phys. JETP **56** (1982) 299.
9. F. Lederer, U. Langbein, and H.-E. Ponath, Appl. Phys. B **31** (1983) 69.
10. A. D. Boardman and P. Egan, Phil. Trans. Roy. Soc. A **313** (1984) 173.
11. J. Bergou and M. O. Scully, Acta Phys. Austriaca **57** (1985) 139.
12. U. Langbein, F. Lederer, H.-E. Ponath, and U. Trutschel, Appl. Phys. B **38** (1985) 263.
13. D. Marcuse, Theory of Dielectric Optical Wavequides (New York, Academic Press, 1974).
14. J. Bergou, M. O. Scully, and J. M. O'Hare in preparation.
15. H. Vach, C. T. Seaton, G. I. Stegeman, and I. C. Khoo, Optics Lett. **9** (1984) 238.
16. For reviews, see J. H. Eberly and P. Lambropoulos, **Multiphoton Processes** (Wiley, New York, 1978); G. Mainfray, J. Physique **43**, 2 (1982); J. Morellec, D. Normand, and G. Petite, Adv. At. Mol. Phys. **18**, 97 (1982); S. L. Chin and P. Lambroponlos, **Multiphoton Ionization of Atoms** (Academic, Toronto, 1984).
17. P. Kruit, J. Kimman, M. G. Muller, and M. J. van der Wiel, Phys. Rev. A **28**, 248 (1983).
18. **H. J. Humpert, R. Hippler, H. Schwier, and H. O. Lutz, Proc. of the Advanced Study Institute on "Fundamental Processes in Atomic Collision Physics" 1984, (Plenum, NY, 1985).**
19. **L. A. Lompré, A. L'Huillier, G. Mainfray, and C. Manus, J. Opt. Soc. Am. B2, 1906 (1985).**
20. **U. Johann, T. S. Luk, H. Egger, and C. K. Rhodes, Phys. Rev. A 34, 1084 (1986).**
21. **T. J. McIlrath, P. H. Bucksbaum, R. R. Freeman, and M. Bashkansky, Phys. Rev. 35, 4611 (1987).**
22. **L-A. Lompré, G. Mainfray, C. Manus, and J. Kupersztych, J. Phys. B 20, 1009 (1987).**
23. **Z. Deng and J. H. Eberly, Phys. Rev. Lett. 53, 1810 (1984).**

24. L-A. Lompré, G. Mainfray, C. Manus, and J. Thebault, Phys. Rev. A **15**, 1604 (1977); L-A. Lompré, G. Mainfray and C. Manus, J. Phys. B **13**, 85 (1980).
25. J. Zakrzewski and K. Życzkowski, Phys. Rev. A **36**, 4311 (1987); A. Giusti-Suzor and P. Zoller, Phys. Rev. A **36**, 5178 (1987).
26. See, for example, W. Becker and J. K. McIver, J. Physique **44**, C1-289 (1983); Phys. Reports **154**, 205 (1987).
27. N. M. Kroll and K. M. Watson, Phys. Rev. A **8**, 804 (1973).
28. W. Becker, R. R. Schlicher, and M. O. Scully, Nucl. Phys. A **426**, 125 (1984); E. K. Akhmedov, Sov. Phys. JETP **60**, 884 (1984).
29. R. R. Schlicher, W. Becker, and M. O. Scully, Proc. of the NATO ASI on Nonequilibrium Cooperative Phenomena in Physics and Related Fields, 1983, ed. by M. G. Velarde, (Plenum, NY, 1984).
30. R. V. Jensen, Phys. Rev. A **30** (1984) 386.
31. H. G. Muller, A. Tip, and M. J. van der Wiel, J. Phys. B **16** L 679 (1983); W. Becker, R. R. Schlicher, and M. O. Scully , J. Phys. B **19**, L785 (1986); P. H. Bucksbaum, R. R. Freeman, M. Bashkansky, and T. J. McIlrath, J. Opt. Soc. Amer. B **4**, 760 (1987).